UNIVERSIDADE
BEIRA INTERIOR

Performance Comparison of a Scramjet with an Oblique Detonation Wave Engine

Inês Isabel Ribeiro Pereirinha

Dissertação para obtenção do Grau de Mestre em

Engenharia Aeronáutica

(mestrado integrado)

Orientador: Prof. Doutor Francisco Miguel Ribeiro Proença Brojo

outubro de 2022

Declaração de Integridade

Eu, Inês Isabel Ribeiro Pereirinha, que abaixo assino, estudante com o número de inscrição 39874 de/o Mestrado Integrado em Engenharia Aeronáutica da Faculdade de Engenharia, declaro ter desenvolvido o presente trabalho e elaborado o presente texto em total consonância com o **Código de Integridades da Universidade da Beira Interior**.

Mais concretamente afirmo não ter incorrido em qualquer das variedades de Fraude Académica, e que aqui declaro conhecer, que em particular atendi à exigida referenciação de frases, extratos, imagens e outras formas de trabalho intelectual, e assumindo assim na íntegra as responsabilidades da autoria.

Universidade da Beira Interior, Covilhã 06/10 /22

Assinado por: **Inês Isabel Ribeiro Pereirinha**
Num. de Identificação: 15330994
Data: 2022.10.06 22:04:29 +0200

Dedicated to my family and friends

Agradecimentos

A realização deste trabalho só foi possível com o imprescindível apoio e cooperação de todos os que me acompanharam, aos quais deixo aqui o meu mais sincero agradecimento.

Ao meu orientador, Professor Francisco Brojo, pelo acompanhemento, apoio e orientação que me deu durante a realização deste trabalho. Para além disso, gostaria também de agradecer a sua disponibilidade para discutir as minhas questões, bem como as suas críticas construtivas que muito me ajudaram a melhorar esta dissertação.

Aos amigos que fiz ao longo deste percurso, que sempre me ajudaram durante estes 5 anos e que tornaram mais suportáveis os momentos menos bons. Além do mais, também lhes agradeço todos os bons momentos e aventuras.

À Carolina, à Leonor e à Inês, as minhas amigas de casa, que apesar da distância, sempre senti que estavam perto.

Por fim, aos meus Pais e à minha Irmã, a melhor família que poderia ter, e que sempre fez tudo para me ajudar. Sem o vosso apoio incondicional teria sido impossível chegar aqui.

Resumo

Hypersonic airbreathing propulsion tem a capacidade de revolucionar quer a indústria da aviação, quer a indústria espacial. Para além dos motores pertencentes a esta classe não necessitarem de transportar o oxidante para a combustão, quando comparados com o motor foguete, oferecem um impulso específico superior a elevados números de Mach. Assim, durante muito tempo, o foco da propulsão hipersónica foi o scramjet. No entanto, outros conceitos têm vindo a ser propostos que parecem ter um melhor desempenho, como é o caso dos motores de detonação oblíqua, ODWE.

Esta tese apresenta o desenvolvimento de um código que visa calcular e comparar o desempenho de um motor scramjet com um motor de detonação oblíqua (ODWE). O estudo realizado é unidimensional e as estações consideradas para os motores são admissão/compressão, combustão e expansão. Para o motor scramjet a *stream thurst analysis* é implementada, permitindo uma análise mais precisa quando comparada a outras metodologias unidimensionais. Além disso, a combustão é considerada quer a pressão constante, quer em área constante. Quanto ao motor de detonação oblíqua, o modelo matemático apresentado por Pratt (1991) é implementado, mas considerando a eficiência da combustão.

Dadas condições básicas de operação, tais como altitude e número Mach, o código calcula as propriedades necessárias em cada estação. Assim, os parâmetros de desempenho relevantes podem ser estimados, dando ao leitor uma ideia sólida de como os motores se comparam ao nível do seu desempenho. São também apresentados e analisados os resultados de um estudo específico em que se queima estequiométricamente H2/ar. Conclui-se que o motor de detonação oblíqua tem melhor desempenho do que o scramjet, o que justifica todos os esforços de pesquisa em torno deste motor, e também no uso das detonações em diferentes sistemas de propulsão.

Palavras-chave

Propulsão hipérsónica, scramjet, scramjet de pressão constante, scramjet de área constante, motor de detonação oblíqua, performance, detonação, análise *stream thrust*.

Abstract

Hypersonic airbreathing propulsion has the ability to revolutionise both the industry of aviation and space launchers. Apart from not needing to carry the oxidizer needed for combustion, when compared to rockets, this class of engines often offers higher specific impulse at high Mach numbers. For a very long time, the focus of hypersonic airbreathing propulsion was on the scramjet engine. Nevertheless, other concepts have been proposed that seem to outperform the first one. An example of this is the oblique detonation wave engine, ODWE.

This thesis presents the development of a code that aims to calculate and compare the performance of a scramjet engine with an oblique detonation wave engine (ODWE). The study conducted is one-dimensional and the stations considered for the engines are air intake/compression, combustion and expansion. For the scramjet engine, stream thrust analysis is implemented, allowing for a more accurate analysis when compared to other one-dimensional methods. Moreover, both constant pressure and constant area burner are considered. As for the oblique detonation wave engine, the mathematical model presented by Pratt (1991) is implemented, but considering the efficiency of combustion.

Given basic operation conditions, such as altitude and freestream Mach number, the code calculates the necessary properties at each station and all relevant performance parameters can be estimated, giving great insight into how the engines compare regarding their performance. Results of a specific case study burning H_2/air at stoichiometric conditions are presented and analysed. The oblique detonation wave engine is found to have overall better performance than the scramjet engine, which justifies all the research efforts around this engine and the overall use of detonations on different propulsion systems.

Keywords

Hypersonic propulsion, scramjet, constant pressure scramjet, constant area scramjet, oblique detonation wave engine, performance, detonation, stream thrust analysis.

Contents

List of Figures

List of Tables

Nomenclature

A	Area	m^2
a	Speed of sound	$m \cdot s^{-1}$
C_f	Burner skin friction coefficient	-
C_p	Specific heat at constant pressure	$J \cdot kg^{-1} \cdot K^{-1}$
F	Uninstalled thrust	N
$\frac{F}{\dot{m}_0}$	Specific thrust	$N \cdot s \cdot kg^{-1}$
f	Fuel/Air ratio	-
g	Acceleration of gravity	$m \cdot s^{-2}$
g_0	Acceleration of gravity at the surface of Earth	$m \cdot s^{-2}$
h	Height	m
	Enthalpy per unit mass	$J \cdot kg^{-1}$
h_f	Absolute sensible enthalpy of fuel entering combustor	$J \cdot kg^{-1}$
h_{PR}	Heat of reaction	$J \cdot kg^{-1}$
I_{sp}	Specific impulse	s
M	Mach number	-
$\dot{m}$	Mass flow rate	$kg \cdot s^{-1}$
p	Absolute pressure	Pa
R	Gas constant	$J \cdot kg^{-1} \cdot K^{-1}$
S	Specific fuel consumption	$kg \cdot s^{-1} \cdot N^{-1}$
Sa	Stream thrust function	$N \cdot s \cdot kg^{-1}$
T	Absolute temperature	K
Q	Energy added per unit mass	$J \cdot kg^{-1}$
$\tilde{q}$ or $\tilde{Q}$	Dimensionless ODW heat flux	-
T_{ign}	Self-ignition temperature	K
V	Absolute velocity	$m \cdot s^{-1}$
Greek letters		
β	ODW angle	deg
γ	Ratio of specific heats	-
η	Efficiency	-

θ	Wedge angle	deg
λ	Lapse rate	$K \cdot m^{-1}$
π_c	Total pressure ratio	-
ρ	Density	$kg \cdot m^{-3}$
ϕ	Fuel/air equivalence ratio	-
φ	Ratio of burner entry temperature to freestream temperature	-

Subscripts

b	Combustion process
c	Compression process
$Ch.J$	Chapman-Jouguet condition
e	Exit or exhaust
	Expansion process
f	Fuel
fx	Axial fuel injection
KE	Kinetic energy
p	Propulsive
o	overall
OD	On-design
$ratio$	Ratio of downstream to upstream conditions
st	Stoichiometric condition
t	Total or stagnation condition
th	Thermal
w	Wall
0	Freestream conditions
1	Upstream of a process
$1n$	Normal component upstream of a process
2	Downstream of a process
$2n$	Normal component downstream of a process
3	Burner entry/compression exit conditions
4	Burner exit/nozzle entry conditions
10	Nozzle exit conditions

Superscripts

o	Reference temperature for absolute enthalpy

List of Abbreviations

ODWE	Oblique Detonation Wave Engine
ODW	Oblique Detonation Wave

Chapter 1

Introduction

1.1 Motivation

The interest in hypersonic airbreathing propulsion has been growing over the years. This technology can revolutionise the aerospace field not only by powering vehicles to fly faster than five times the speed of sound, but also by potentially creating a new class of flight vehicles that can allow for a faster access to space, as well as faster commercial air travel.

Over the years, scramjet engines have been highly studied in order to unleash the potential of hypersonic airbreathing propulsion. Compared to rockets, one can easily point out the advantages of scramjet technology. Scramjets not only usually produce higher specific impulse than rockets, but also do not need to carry oxidizer for combustion. This means heavier payload can be transported, making flights more cost efficient. Nevertheless, other propulsion devices have been proposed for hypersonic flight, such as the Oblique Detonation Wave Engine. This engine replaces the diffusive combustion of scramjets with an oblique detonation, allowing for a shorter and simpler combustor design. Additionally, it is expected to have better thrust performance than traditional scramjet engines.

Although there is still a long way to go in hypersonic airbreathing propulsion, the research being conducted in the field is of utmost importance. The ultimate motivation behind this dissertation is to better understand and compare the performance of these two engines, and the role they each play in the future of hypersonic flight.

1.2 Objectives

The goal of this dissertation is to describe the development of a numerical tool that can successfully compare the performance of an oblique detonation wave engine with a scramjet engine. Both constant pressure and constant area scramjet combustion will be studied in order to also provide a good picture of how it affects the performance of the scramjet engine.

The tool should be able to optimize the inlet geometry for a given Mach number, and then calculate engine performance for a specified range of hypersonic Mach numbers. This tool can also be useful for vehicle preliminary design, as the airframe of a hypersonic vehicle is highly influenced by engine geometry. This means that with a preliminary performance assessment, one can have an estimation of the overall vehicle geometry. Results are delivered promptly, allowing for testing of various input conditions and quickly assessing their influence on overall engine performance.

A test case will be implemented and results will then be presented and analysed in order to have a clear view of how both engines perform in specified conditions.

1.3 Dissertation Outline

The present dissertation is organised in five chapters. They are the following: Introduction; Literature Review; Methodology; Results; and Conclusion.

The first chapter describes what is the motivation behind the study conducted, the objectives it aims to accomplish and also gives the reader a better insight into how the dissertation is organised. The Literature Review is focused on providing a clear understanding of both engines being analysed, and the research that has been done to make advances in hypersonic airbreathing propulsion. The literature referenced in this chapter is the foundation that led to the development of the current project. The Methodology describes the approach that was taken to conduct the project, as well as the mathematical formulation of all equations applied. It also provides a good insight into how the Python code was developed and how it works. The Results chapter is focused on presenting the output the code produces after doing the calculations for the specified case study. The output is analysed for a better understanding of how the performance compares, as well as what influences it. The Conclusion presents the main outcomes of the project, as well as a suggestion for future work that aims to mature the technology development in hypersonic airbreathing propulsion.

Chapter 2

Literature Review

2.1 Hypersonic Airbreathing Propulsion

Hypersonic airbreathing propulsion technology is maturing fastly with the aim to transform and make hypersonic flight more accessible. Despite the fact that practical hypersonic airbreathing propulsion systems have not been developed despite more than 40 years of research, substantial technological improvements have lately been made [1]. The most common engines associated with hypersonic airbreathing propulsion are scramjets and ramjets.

Nevertheless, other engine configurations have been proposed, such as the Oblique Detonation Wave Engine. The key difference of this engine is the fact that combustion happens by detonation instead of deflagration. According to Ashford et al. [2], several studies have found acceptable performance of this engine in the Mach range of 6-22. Additionally, according to Jiang et al. [3] the scramjet combustion mode cannot meet the thrust needs of hypersonic vehicles. The reason behind this is the fact that scramjet thermal efficiency drops as the Mach number increases. Although, ODWE's thermal efficiency also drops as the Mach number increases, it is still higher than the thermal efficiency of the scramjet.

It is also important to note that major research is still required in the field of hypersonic airbreathing engines, since these engines have a high starting Mach number. This means that both scramjets and ODWEs are dependent on other engines to take-off and accelerate to the starting Mach number, which increases the complexity of the system.

2.2 Scramjet

With the aim of establishing a definition of the scramjet engine, one needs to understand the ramjet engine first. Unlike a gas turbine, ramjets have no rotating machinery. Compression is attained through shock waves that are usually generated by the forebody of the vehicle. In a ramjet, the flow is decelerated to subsonic speeds after compression, mean-

ing the combustion is subsonic. According to Heiser and Pratt [4] this is efficient in the Mach range of 3-6. Nevertheless, as the Mach number increases, it is no longer efficient to decelerate the air to subsonic speeds, so combustion needs to be supersonic. What results from this, is a supersonic combustion ramjet, also called scramjet. A two-dimensional schematic diagram of the scramjet engine is shown in Figure 2.1.

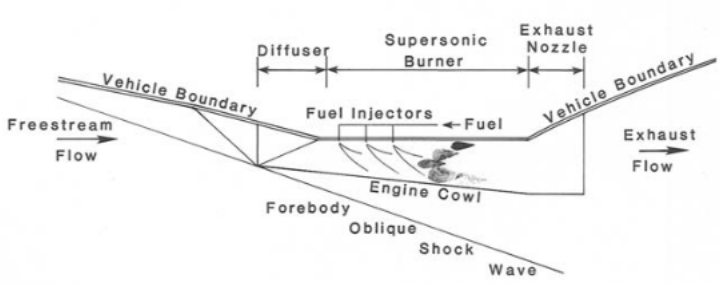

Figure 2.1: Two-dimensional schematic diagram of a scramjet engine [4].

Scramjet engines have been highly studied but there are still many technical challenges that need to be overcome besides the high starting Mach number. For example, according to Heiser et al. [4] it is necessary to assure not only stable, but also efficient mixing and combustion in a supersonic flow within a combustion chamber with an adequate length. Additionally, these engines operate in an environment of extreme temperature and pressure. Thus, it is also a challenge to assure the structural integrity that is of utmost importance in order to have a reusable engine. Unfortunately, the challenges do not end here, and creating the analytical tools that allow for confident engine design control and accurate behaviour prediction is also a concern.

Research to solve these issues has been conducted. As an example, Roberts [5] has studied the possibility of lowering the scramjet starting Mach number to 3.50. Moreover, Roberts also includes important insights on fuel and design choices that help to attain the goal of the study, as well as focusing on how to improve scramjet performance.

Tsujikawa et al. [6] have proposed a performance analysis with a quasi-one-dimensional flow model, while Rolim et al.[7] uses the stream thrust analysis to assess scramjet performance for an acceleration mission from 2 to 3 km/s. Additionally, the last authors also present important results of design parametric studies.

Tran [8] has developed a one-dimensional analysis program for scramjet and ramjet flowpaths. A new one-dimensional MATLAB-based model called VTMODEL is created, and it

includes modelling capabilities that allow for extensive examination of the flow dynamics inside the combustor.

2.2.1 Deflagration

Given the content of the present work, it is also beneficial to define deflagrations, as it characterizes combustion in a scramjet. According to Diéguez et al. [9], deflagration can be defined as the passage of a flame front as a subsonic wave through a combustible mixture in relation to an unreacted medium.

In accordance with Lee et al. [10], by diffusing heat and mass from the flame zone, a deflagration wave spreads and ignites the reactants up ahead. Heat and mass diffusivity control the propagation speed. Also, the reaction rate that preserves the flame's steep gradient also affects the diffusion flux.

2.3 Oblique Detonation Wave Engine

According to Pratt et al. [11], it was back in 1946 when Roy [12] suggested the use of normal detonation waves for hypersonic vehicle propulsion. Further studies concluded thermodynamic feasibility, nevertheless, detonation stabilization seemed difficult and appeared to require variable engine geometry. In addition to that, downstream of a normal detonation, just like downstream of a normal shock, the Mach number is subsonic. This would result in extreme temperature and pressure that would ultimately lead to dissociation.

It was Dunlap et al. [1] that later suggested the implementation of oblique detonations instead of normal detonations, as it allows for supersonic flow throughout the burner, similar to the scramjet engine. This would lead to invariable engine geometry and motivated the appearance of the Oblique Detonation Wave Engine.

With only one glimpse, one can struggle to find the difference between scramjets and ODWEs by only looking at their geometries. Nevertheless, in Figure 2.2 one can spot the wedge that exists in the combustor.
An oblique detonation is generated when the supersonic fuel/air mixture flows over the wedge [14]. Several advantages arise by having a detonation-based combustion instead of diffusive combustion. Valorani et al. [15] stated several, such as the possibility of delaying

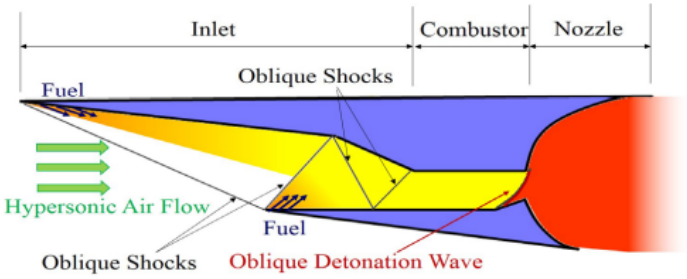

Figure 2.2: Two-dimensional schematic diagram of an Oblique Detonation Wave Engine [13].

the starting Mach number of rocket operation. Logically, this would save weight as less oxidizer would have to be transported, increasing vehicle payload. Additionally, ODWEs allow for a much shorter burner when compared to scramjets [11].

Moreover, ODWEs can have a simpler and shorter compression system, as the temperature ratio across compression can be lower due to the high temperatures and pressures that occur in the burner because of the detonation. Rosato et al. [16] state that the detonation can effectively increase thermodynamic cycle efficiencies from approximately 10 to 20 % when compared to typical cycles that are based on diffusive burning. Dunlap et al. [1] also stated that by using a detonation, there is no need for ignition devices, thus reducing engine complexity.

Based on the advantages these engines seem to offer when compared to scramjets, several researchers have embraced the topic and made great contributions to mature the technology. Jiang et al. [3] propose a standing oblique detonation ramjet to replace diffusive burning. The engine is developed successfully and the study also concludes the engine model can work steadily. Additionally, it confirms that an oblique detonation can be stationary, as well as controllable in the burner.

Pratt et al. [11] have developed the mathematical model of the detonation that is used in this dissertation to analyse and determine burner conditions after the detonation. Additionally, it clarifies the interactions between thermodynamic, chemical-kinetic, and gas dynamic considerations that end up determining the envelope of operating conditions that assure stable ODW with an acceptable pressure loss.

Ashford et al. [2] conducted a performance prediction study, where the performance of an oblique detonation wave engine is compared to diffusive scramjet engines. Both constant

area and constant pressure scramjets are considered, as well as perfect and real gas models are employed. Besides, frozen and equilibrium nozzles are also analysed, providing a good insight into how it affects engine performance. Additionally, it is verified that the ODWE allows for a smaller engine. For the specific case of Mach 10 cruising configuration, it was concluded that the ODWE could reduce engine length by 50 %.

Cambier et al. [17] developed a code for simulating supersonic combustion and used it to perform flow calculations related to the concept behind the oblique detonation wave engine (ODWE). The code was applied to the simulations of detonations generated by a wedge placed in a supersonic stream of stoichiometric and uniformly mixed hydrogen-air. It was concluded that attached detonations were possible.

2.3.1 Detonation

Detonations are supersonic combustion waves that propagate through a reactive gaseous mixture of fuel and oxidizer [18]. In order to give a more precise definition and cite Heiser and Pratt, "Detonation is said to occur when a shock wave-induced combustion wave follows so closely behind the igniting shock wave that the two waves are pressure-coupled". They can be classified according to whether the Mach number downstream of the detonation is subsonic, sonic or supersonic. If the Mach number downstream is subsonic, the detonation is said to be overdriven, if it is sonic, then it is a Chapman-Jouguet detonation and lastly, if it is supersonic, then the detonation is classified as underdriven. Additionally, similarly to oblique shocks, for the same wedge angle, an oblique detonation can have a weak or a strong shock solution.

A generalised diagram of oblique detonation wave angle as function of deflection angle and heat addition, for constant upstream conditions and addressing the classifications of the different possible downstream flowfields, is given in Figure 2.3.
Special attention should be paid to the Chapman-Jouguet locus, which is the point of minimum wave angle on each locus of states for a given $\tilde{q}>0$. Strong overdriven oblique detonation waves, like regular strong oblique shock waves, are linked to static pressure rises that are so great that they detach and are hence unnatural. The weak overdriven detonation waves, which are restricted by the Chapman-Jouguet angle and the detachment angle, are therefore the region of interest for ODWs, as shown in Figure 2.3. The underdriven detonations are not suitable for ODWEs because the normal component of the downstream

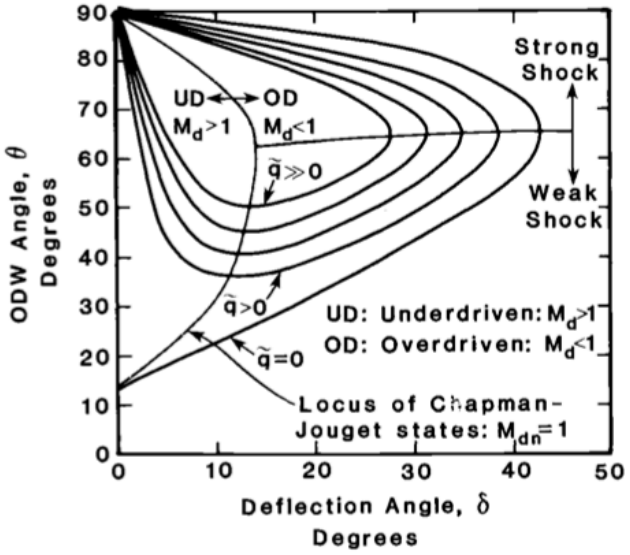

Figure 2.3: Generalised form of oblique detonation wave angle as function of deflection angle and heat addition, for constant upstream conditions [4].

Mach number is supersonic. Thus, the normal component of the downstream Mach number needs to be either sonic or subsonic to assure the ODW is attached and stable.

2.3.1.1 Chapman-Jouguet Theory

Chapman (1899) and Jouguet (1905) established what is the earliest theory on detonations [19]. The theory describes the detonation wave as a hydrodynamic discontinuity across which energy release occurs, and assumes it is stable, planar, and one-dimensional.

It is also worth mentioning the Hugoniot relationship, where subscripts 1 and 2 stand for before and after the detonation, respectively.

$$h_2 - h_1 = \frac{1}{2}(p_2 - p_1)(1/\rho_1 + 1/\rho_2) \quad \textbf{(2.1)}$$

Using the Hugoniot relationship, the Hugoniot curve can be plotted, which allows to determine the possible solutions for state 2, given a particular state 1 and energy release. An exemplifying plot of this curve can be seen below, in Figure 2.4.
Regions I and II coincide with supersonic waves (detonations). On the other hand, regions IV and V relate to subsonic waves, also known as deflagrations.

The actual propagation speed of deflagrations is determined by the combustion wave's

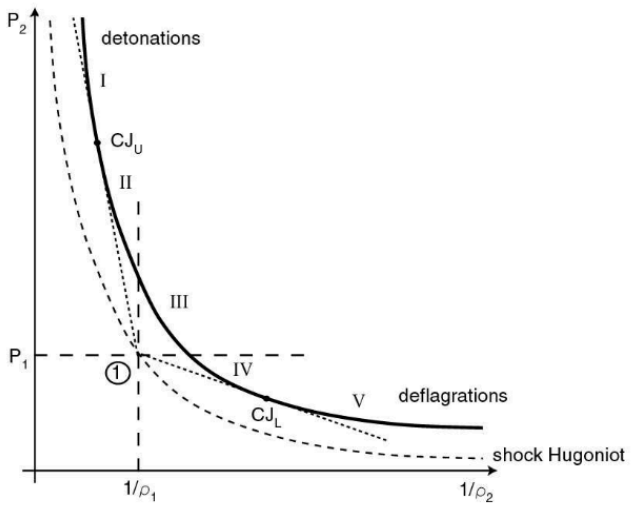

Figure 2.4: Hugoniot curve [19].

structure, as well as turbulent and diffusive transport processes. On the other hand, for detonations, gas dynamic considerations appear to be sufficient to predict the wave propagation speed without regard to the wave's actual structure. Separately, these were the conclusions Chapman and Jouguet came to, suggesting that detonations travel at the very minimum velocity for all the solutions on the detonation branch [19]. Looking into figure 2.4, one can easily see that there are two Chapman-Jouguet points, the upper and the lower. The upper is on the detonation branch, whereas the lower is on the deflagration branch. Here the point of particular interest for ODWE applications is the upper Chapman-Jouguet point, as it corresponds to the detonation branch and is the point of minimum entropy and minimum total pressure loss [11].

2.3.1.2 ZND Model

The ZND detonation model is a one-dimensional, inviscid and steady representation of the explosive detonation process. The term comes from the fact that it was independently proposed during World War II by Werner Döring, John von Neumann, and Y. B. Zel'dovich. The model defines a supersonic detonation combustion wave as a shock front that is immediately followed by an induction zone, which is then followed by a reaction front [18]. For better understanding, Figure 2.5 displays a schematic diagram of the ZND detonation model, as well as a profile of temperature, pressure and density through the detonation wave.

A thermally almost dormant region known as the induction zone is where shocked gas molecules split apart to create active radicals. The shocked reactants' temperature and

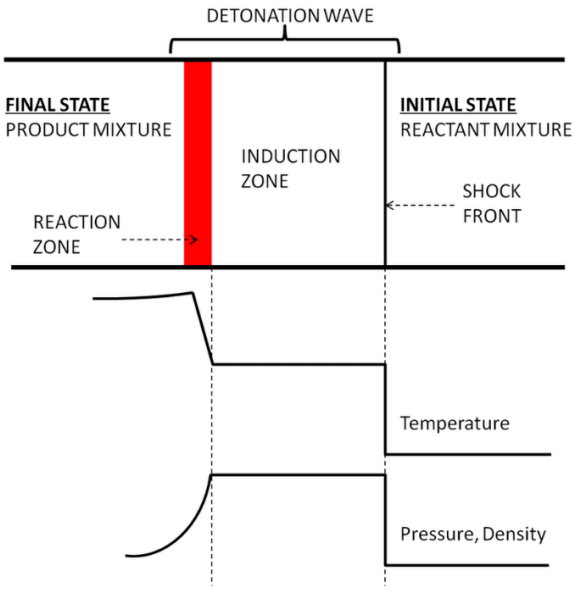

Figure 2.5: Schematic of the ZND detonation model, along with a profile of temperature, pressure, and density across the detonation wave [18].

pressure are essentially constant in this situation. Rapid exothermic reactions that transform reactants into end products start when there is a sufficient amount of these active radicals created. As the gas expands, the exothermic reactions in the reaction zone raise the temperature while lowering the pressure and density.

Although it is now known that detonations are not defined accurately by this model, it is still important to mention it, as it was of utmost importance back in the days for providing a very good understanding of the propagation mechanism, as well as the internal structure of the detonation wave. Additionally, it eventually led to what is known in the area in the present day.

For a more accurate understanding of detonations, and referring to Lee [10], a detonation wave has a three-dimensional cellular structure, instead of the one-dimensional structure proposed by the ZND model. The same author states an unsteady behaviour of the detonation fronts, which has been revealed with the development of cameras in the 1920s and 1930s.

Chapter 3

Methodology

In this chapter, the methodology used to develop the tool is described. Some important considerations to mention are: no isolator will be considered for the scramjet engine, so the on-design Mach number should not be less than 8 [20]. Additionally, only altitudes in the range of 0 to $32\,km$ are accepted.

With the purpose of establishing a reference for the numbering of engine stations, Figure 3.1 follows below, with a generic representation of engine geometry.

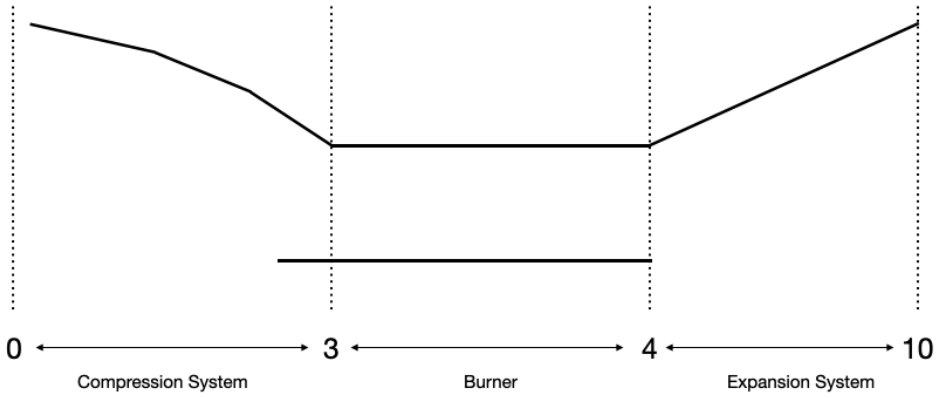

Figure 3.1: Generic representation of engine geometry for station numbering reference.

3.1 Atmosphere Model

In order to study engine performance at various altitudes, the model of the International Standard Atmosphere is implemented. This model is accepted internationally and was proposed in 1952 by the International Civil Aviation Organisation (ICAO). The code receives as input the altitude (from $0\,km$ to $32\,km$) and all important properties are calculated.

To calculate the temperature within the troposphere, the following equation is imple-

mented:

$$T = T_0 - 6.5\frac{h(m)}{1000} \quad (3.1)$$

where T_0 is $288.15\,K$. From the end of the troposphere to an altitude of 20 km, the temperature remains constant and equals $216.65K$. Above the altitude of 20 km and up to $32\,km$, the temperature is given by

$$T = T_{20km} + (h(m) - 20000)10^{-3} \quad (3.2)$$

where T_{20km} is $216.65\,K$. The following property to be addressed is the pressure. To calculate it within the troposphere, the equation below is used:

$$p = p_0 \left(\frac{T}{T_0}\right)^{\frac{-g_0}{R\lambda}} \quad (3.3)$$

where p_0 is $101325\,Pa$, R is $287.05307\,Jkg^{-1}K^{-1}$, λ is $-6.5\times10^{-3}\,K\,m^{-1}$ and g_0 is $9.80665\,m\,s^{-2}$. On the other hand, from 11 to $20\,km$ of altitude, pressure can be obtained through

$$p = p_{11km}e^{\frac{-g_0(h-11000)}{RT_{11km}}} \quad (3.4)$$

where p_{11km} is $22632.06\,Pa$ and T_{11km} is $216.65\,K$. From 20 to $32\,km$ of altitude, the equation implemented is the following:

$$p = p_{20km}\left(\frac{T}{T_{20km}}\right)^{\frac{-g_0}{R\lambda}} \quad (3.5)$$

where p_{20km} is $5474.89\,Pa$, T_{20km} is $216.65\,K$ and λ is $1 \times 10^{-3}\,K\,m^{-1}$.

The following property to be considered is the speed of sound, which can be calculated via

$$a = \sqrt{\gamma RT} \quad (3.6)$$

where $\gamma = 1.4$. Lastly, to calculate the acceleration of gravity for a specific altitude, the following equation is implemented

$$g = g_0\left(\frac{6371000}{6371000 + h}\right)^2 \quad (3.7)$$

where g_0 is $9.80665\,m\,s^{-2}$.

3.2 Compression System

The compression system affects engine performance tremendously. Several factors need to be taken into consideration when designing it to assure that the necessary cycle temperature ratio is provided, but with maximum compression efficiency, as well as minimum entropy increase. Factors that need to be taken into account include type of compression (internal, external or mixed), number and type of shock waves, as well as the size of the final inlet.

For the present work, the engines compared have the very same compression system. Although the engines are different, in light of the goal of this study, which is to compare their performance, this is considered the best approach.

Additionally, the following assumptions are made for the compression system design: one-dimensional flow, air is a calorically perfect gas, inviscid, and heat transfer to or from the wall is neglected. These assumptions are considered appropriate for quickly assessing engine performance. To further refine the geometry, a more complex approach should be implemented.

3.2.1 Inlet Type

The inlet type selected was based on the work of Quan et al. [21]. Internal compression inlets generate a lot of drag because of their shape, and integrating them with the rest of the vehicle is difficult. Furthermore, because of the intricate structure of the flowfield and the requirement for a changeable shape to create stable flow, the design of the internal compression inlet is quite challenging. In an external compression inlet, flow must enter the combustor at a significant angle to the freestream flow in order for all oblique shocks to be outside the entrance throat. This requires the inlet cowl to not be positioned parallel to the freestream flow, which leads to a significant increase in cowl drag. External compression inlet is not a popular option for scramjet intake design because of this drawback. These issues can be solved by a mixed compression inlet, which is also the most popular within hypersonic airbreathing propulsion, hence this is the type that is used in this project. Additionally, the engine cowl angle and amount of compression are ”decoupled” by mixed compression systems, which can lead to a cowl that is parallel to the freestream flow [4]. A representation of a mixed compression inlet is present in Figure 3.2.

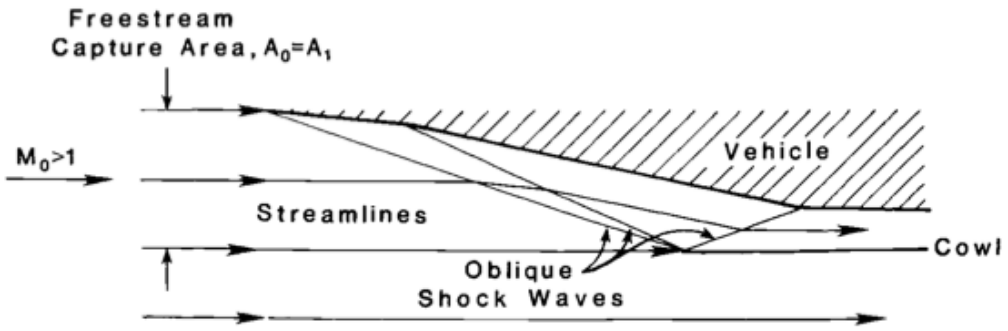

Figure 3.2: Representation of a mixed compression inlet [4].

3.2.2 Number of Oblique Shocks

The next step is to determine how many oblique shock waves should be generated by the inlet to assure the desired cycle temperature ratio with great efficiency and minimum entropy increase. Additionally, the inlet should provide acceptable performance in off-design conditions and should be of an acceptable length.

For the code being developed in this project, the design of the compression system is conducted based on the desired cycle temperature ratio T_3/T_0. Additionally, from all the possibilities for the compression system design, it was decided to assure that all oblique shock waves need to impart equal amounts of geometric turning of the flow, and at design point operation, the shock-on-lip condition is verified [4]. Looking into Figure 3.3, one can conclude that a system of 4 oblique shock waves seems to be the wisest choice. Increasing the number of oblique shocks would lead to a longer compression system and more off-design complications are likely to appear [5]. For this reason, a system of 4 oblique shock waves is considered for this study.

3.2.3 Mathematical Model

As for the mathematical model implemented, in order to calculate the properties of the flow after each shock, the traditional oblique shock equations in 3.8,3.9,3.10, 3.11 and 3.12 were applied.

$$p_{\text{ratio}} = 1 + \frac{2\gamma_0}{\gamma_0 + 1}\left[M^2 \sin^2\beta - 1\right] \quad (3.8)$$

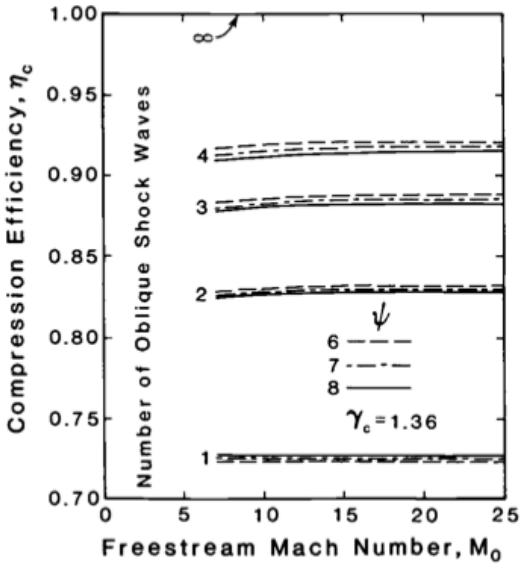

Figure 3.3: Adiabatic compression efficiency as a function of freestream Mach number, static temperature ratio, and number of oblique shock waves [4].

$$\rho_{\text{ratio}} = \frac{(\gamma_0 + 1)\, M^2 \sin^2 \beta}{2 + (\gamma_0 - 1)\, M^2 \sin^2 \beta} \quad (3.9)$$

$$T_{\text{ratio}} = p_{\text{ratio}} / \rho_{\text{ratio}} \quad (3.10)$$

$$\tan \theta = \frac{2 \cot \beta \left[M^2 \sin^2 \beta - 1 \right]}{M^2 \left[\gamma_0 + \cos(2\beta) \right] + 2} \quad (3.11)$$

$$M_{\text{ratio}} = \frac{1}{M} \left(\frac{2}{\gamma_0 - 1} + M^2 \sin^2 \beta \right)^{1/2} \left(\frac{2\gamma_0 M^2 \sin^2 \beta}{\gamma_0 - 1} - 1 \right)^{-1/2} \quad (3.12)$$

Additionally, η_c and η_{KE} are determined via the following equations taken from [4]

$$\pi_c = \frac{p_{t3}}{p_{t0}} = \frac{p_3}{p_0} \left(\frac{1}{\varphi} \right)^{\gamma_c/(\gamma_c - 1)} \quad (3.13)$$

$$\eta_c = \frac{\varphi - \left(\frac{1}{\pi_c}\right)^{(\gamma_c - 1)/\gamma_c}}{\varphi - 1} \quad (3.14)$$

$$\eta_{KE} = 1 - \frac{2}{(\gamma_c - 1)\, M_0^2} \left\{ \left(\frac{1}{\pi_c}\right)^{(\gamma_c - 1)/\gamma_c} - 1 \right\} \quad (3.15)$$

where $\varphi = T_3/T_0$.

3.3 Combustion System

For the combustion study, it is considered that combustion starts with air and fuel completely mixed. The chemical equation that represents the complete combustion of air and a hydrocarbon fuel is called the stoichiometric equation and is given by [4]

$$\begin{aligned} \mathrm{C}_x\mathrm{H}_y + \left(x + \frac{y}{4}\right)\left(\mathrm{O}_2 + \frac{79}{21}\,\mathrm{N}_2\right) \\ \rightarrow x\mathrm{CO}_2 + \frac{y}{2}\mathrm{H}_2\mathrm{O} + \frac{79}{21}\left(x + \frac{y}{4}\right)\mathrm{N}_2 \end{aligned} \quad (3.16)$$

The stoichiometric fuel/air ratio can be calculated via

$$f_{st} = \frac{36x + 3y}{103(4x + y)} \quad (3.17)$$

In the case of non-stoichiometric mixtures, it is useful to define the equivalence ratio, which is the ratio of real fuel/air ratio to stoichiometric fuel/air ratio. This is given by

$$\phi \equiv \frac{f}{f_{\mathrm{st}}} \quad (3.18)$$

According to Heiser and Pratt [4], as a general rule, for combustion to take place within a reasonable timescale, the equivalence ratio must be in the range of 0.2 to 2.

In this project, the selected fuel is H_2. From the fuels present in Table 3.1, it can be concluded that H_2 has the highest heating value. Additionally, its self-ignition temperature

is also the highest. The major drawback when selecting H_2 is its low density, which ultimately leads to the necessity of lots of space to store it in the aircraft. Nevertheless, lots of research has been conducted to overcome this issue, such as solutions to store it as a liquid, requiring cryogenic temperatures [4] [7].

Table 3.1: Properties of several fuels, where ρ is for standard conditions and T_{ign} is for standard conditions and $1\,atm$ [7].

Fuel	$h_{PR}\,[MJ/kg]$	$\rho\,[kg/m^3]$	$T_{ign}\,[K]$	f_{st}
H_2	119.96	0.08	845.15	0.02913
CH_4	50.01	0.65	810.15	0.05825
C_2H_6	47.49	1.22	745.15	0.06241
C_3H_3	46.3	1.79	743.15	0.06408
C_4H_{10}	45.74	2.36	693.15	0.06497

3.3.1 Scramjet

To analyse scramjet combustion, it was decided to study both constant area and constant pressure combustion. For certain burner entrance conditions, constant area scramjet usually produces the highest specific impulse [22]. On the other hand, it is stated by Ferri [23] that a constant pressure process has a higher performance than constant area combustion, for a given maximum engine pressure. It is also known that an absolutely constant pressure burner is not viable, taking into account the manufacturing capabilities of the present day [4].

To analyse both of these processes, the stream thrust analysis is implemented. This method is selected, as it accounts for phenomenon that other one-dimensional flow analysis methods, such as the Thermodynamic Closed Cycle Analysis or the First Law Analysis, do not account for. In light of this, it should be the most accurate method, when compared to the others mentioned, as it takes into account "the mass, momentum, and kinetic energy fluxes contributed by the fuel, the geometry of the burner, and exhaust flows that are not matched to the ambient pressure" [4].

3.3.1.1 Constant Pressure

For constant pressure combustion, the following equations are implemented [4]:

1. V_4

$$V_4 = V_3 \left\{ \frac{1 + f \cdot \frac{V_{fx}}{V_3}}{1+f} - \frac{C_f \cdot \frac{A_w}{A_3}}{2(1+f)} \right\} \quad (3.19)$$

2. T_4

$$T_4 = \frac{T_3}{1+f}\left\{1 + \frac{1}{C_{pb}T_3}\left[\eta_b f h_{PR} + f h_f + f C_{pb} T^\circ + \left(1 + f \cdot \frac{V_f^2}{V_3^2}\right)\frac{V_3^2}{2}\right]\right\} - \frac{V_4^2}{2C_{pb}} \tag{3.20}$$

It should be noted that h_f (absolute sensible enthalpy of fuel entering the combustor) is neglected as it is usually less than h_{pr} [4].

3. A_3/A_4

$$\frac{A_4}{A_3} = (1+f)\cdot\frac{T_4}{T_3}\cdot\frac{V_3}{V_4} \tag{3.21}$$

3.3.1.2 Constant Area

For constant area combustion, the following equations are implemented [4]:

1. V_4

$$V_4 = \frac{-b \pm \sqrt{b^2 - 4ac}}{2a} \tag{3.22}$$

where,

$$a = 1 - \frac{R}{2C_{pb}} \tag{3.23}$$

$$b = -\frac{V_3}{1+f}\left\{\left(1 + \frac{RT_3}{V_3^2}\right) + f\cdot\frac{V_{fx}}{V_3} - \frac{C_f}{2}\cdot\frac{A_w}{A_3}\right\} \tag{3.24}$$

$$c = \frac{RT_3}{1+f}\left\{1 + \frac{1}{C_{pb}T_3}\left[\eta_b f h_{PR} + f h_f + f C_{pb} T^\circ + \left(1 + f \cdot \frac{V_f^2}{V_3^2}\right)\frac{V_3^2}{2}\right]\right\} \tag{3.25}$$

As one can conclude, for the constant area combustor there are two different solutions for V_4 that lead to very different properties at the exit of the burner. In this project, only the solution which corresponds to the highest V_4 is considered.

2. T_4

$$T_4 = \frac{c}{R} - \frac{V_4^2}{2C_{pb}} \quad (3.26)$$

3. p_4/p_0

$$\frac{p_4}{p_0} = (1+f) \cdot \frac{p_3}{p_0} \cdot \frac{V_3}{V_4} \cdot \frac{T_4}{T_3} \quad (3.27)$$

3.3.2 Oblique Detonation Wave Engine

On chapter 2, it was stated that the types of detonations that can be applied to hypersonic airbreathing propulsion are both the Chapman-Jouguet and the weak overdriven detonations. Additionally, it should be reminded that Chapman-Jouguet detonations correspond to the minimum total pressure loss and point of minimum entropy. Considering this, for on-design conditions the programme should determine which wedge angle generates a Chapman-Jouguet detonation. For the following Mach numbers, a weak overdriven detonation should be assured. Additionally, to prevent pre-ignition in the specific case of burning H_2 under stoichiometric conditions, according to Ashford and Emanuel [2], temperature before the detonation wave should be less than 1000 K. On the other hand, to assure ignition, temperature after detonation should be more than 1000 K. If this condition is not satisfied, the programme will warn the user.

In order to determine the Chapman-Jouguet detonation angle for the design Mach number, the following equation is solved

$$\left(M_{1_n}^2 - 1\right)^2 - 2(\gamma+1)M_{1_n}^2 \tilde{Q} = 0 \quad (3.28)$$

where M_{1n}=$M_1 \sin\beta$ and $\tilde{Q} = \frac{Q\eta_b}{CpT}$.
To find the wedge angle that generates a Chapman-Jouguet detonation at on-design conditions, $\theta_{Ch.J.}$, the following equation is solved.

$$\theta_{\text{Ch.J.}} = \beta_{\text{Ch.J.}} - \tan^{-1}\left[\frac{1+\gamma M_{1_n\,\text{Ch.J.}}^2}{(\gamma+1)M_{1_n\,\text{Ch.J.}}^2 \sqrt{\left(M_1/M_{1_n\,\text{Ch.J.}}\right)^2 - 1}}\right] \quad (3.29)$$

For the remaining Mach numbers in the range to be considered, the detonation angle is determined with Equation 3.30, as the wedge angle is already defined.

$$\tilde{Q} = -\frac{\gamma+1}{2}X^2 M_1^2 \sin^2\beta + \left(1 + \gamma M_1^2 \sin^2\beta\right) X - \left(1 + \frac{\gamma-1}{2} M_1^2 \sin^2\beta\right) \quad (3.30)$$

X is defined below in Equation 3.33. Equations 3.28 and 3.29 were taken from Murthy et al. [24]. Equation 3.30 was taken from Heiser et al. [4].

3.3.3 Post-Detonations Properties

After determining the detonation angles for each Mach number to be studied, the following step is to determine the conditions after the detonation. The methodology was taken from Pratt et al. [11], where fuel and air are assumed to be completely mixed. However, in order to make this approach closer to reality, and to be consistent with the analysis of the scramjet combustion, Equation 3.19 is implemented here as well, in order to estimate the velocity of the fuel/air mixture, after fuel is injected. The temperature of the fuel/air mixture is assumed to be the same as the temperature of the air coming out of the compression system, as the temperature of the fuel is neglected here.

Pressure after the detonation is calculated by

$$p_2 = p_1 + \rho_1 u_{1n}^2 (1 - X) \quad (3.31)$$

and the detonation temperature ratio is determined according to

$$\frac{T_2}{T_1} = 1 + \frac{u_{1n}^2}{2C_p T_1}\left(1 - X^2\right) + \frac{Q\eta_b}{C_p T_1} \quad (3.32)$$

where X is given by

$$X \equiv \frac{\rho_1}{\rho_2} = \frac{u_{2n}}{u_{1n}} = \frac{\tan(\beta - \theta)}{\tan\beta} \quad (3.33)$$

and

$$u_{1n} = u_1 \sin\beta \quad (3.34)$$

$$u_{1t} = u_1 \cos\beta \quad (3.35)$$

$$u_{2n} = u_2 \sin(\beta - \theta) \quad (3.36)$$

$$u_{2t} = u_2 \cos(\beta - \theta) \quad (3.37)$$

3.4 Expansion System

Lastly, the expansion system is analysed. Its ultimate goal is to produce thrust and it can operate underexpanded, overexpanded or ideally [4] [5]. Ideally means the exhaust products of combustion are expanded to the atmospheric pressure through the nozzle, which corresponds to $p_{10}/p_0 = 1$. On the other hand, if the nozzle is operating underexpanded, it means that $p_{10}/p_0 > 1$. Operating in this condition results in a smaller length of the nozzle, which ends up saving weight. Lastly, the overexpanded condition means $p_{10}/p_0 < 1$. This condition does not bring any advantages, as less thrust is produced and the nozzle is bigger than it should be for optimum performance.

For the expansion system analysis, one-dimensional and calorically perfect flow is considered. Additionally, the expansion is considered an adiabatic process and it is assumed that the nozzle is ideal. This means that for all conditions analysed $p_{10}/p_0 = 1$. It is also important to note that with this methodology, frozen flow in the expansion system is assumed. This is usually seen as a lower boundary for performance, meaning that this approach is somewhat conservative when compared with the *shifting equilibrium*. Quoting Forbes and Splinter [25], this last approach assumes that "chemical and phase equilibrium among all combustion species is maintained under the varying pressure and temperature conditions of the nozzle expansion process, the product composition will change. This is known as *shifting equilibrium*, and performance so calculated will be the higher value because the dissociated species that recombine in the nozzle add to the release of chemical energy converted into kinetic energy". This usually represents the higher boundary for

performance.

The mathematical model to calculate properties at station 10 follow below [4]:

$$T_{10} = T_4 \left\{ 1 - \eta_e \left[1 - \left(\frac{p_{10}}{p_0} \cdot \frac{p_0}{p_4} \right)^{(R/C_{pe})} \right] \right\} \quad (3.38)$$

$$V_{10} = \sqrt{V_4^2 + 2C_{pe}\left(T_4 - T_{10}\right)} \quad (3.39)$$

$$\frac{A_{10}}{A_0} = (1+f) \cdot \frac{p_0}{p_{10}} \cdot \frac{T_{10}}{T_0} \cdot \frac{V_0}{V_{10}} \quad (3.40)$$

3.4.1 Performance

Lastly, equations to estimate engine performance are presented here and were taken from Pratt et al. [4]. It is important no note that some of the assumptions listed above are very far from being fulfilled in the real flow. Therefore, it is important to take that into consideration when analysing the results obtained for performance.

3.4.1.1 Specific Thrust

Specific thrust is defined as

$$\frac{\text{Uninstalled thrust}}{\text{Entry air mass flow rate}} = \frac{F}{\dot{m}_0} \quad (3.41)$$

Additionally, using the stream thrust function, one can define the specific thrust as

$$\frac{F}{\dot{m}_0} = (1+f)Sa_{10} - Sa_0 - \frac{R_0 T_0}{V_0}\left(\frac{A_{10}}{A_0} - 1\right) \quad (3.42)$$

where

$$Sa_{10} = V_{10}\left(1 + \frac{RT_{10}}{V_{10}^2}\right) \quad (3.43)$$

and

$$Sa_0 = V_0\left(1 + \frac{RT_0}{V_0^2}\right) \quad (3.44)$$

Therefore, the mass flow rate of air that must enter the engine may be derived directly from Equation 3.42 provided both the uninstalled thrust required for a given operation and the specific thrust of the type of engine to be used are known.

3.4.1.2 Specific Fuel Consumption

The specific fuel consumption is defined as

$$\frac{\text{Fuel mass flow rate}}{\text{Uninstalled thrust}} = S = \frac{\dot{m}_f}{F} \quad (3.45)$$

It can also be defined using the specific thrust, as in the equation below:

$$S = \frac{f}{F/\dot{m}_0} \quad (3.46)$$

3.4.1.3 Specific Impulse

One of the most important performance parameters to be calculated when it comes to engine performance is the specific impulse, as it is able to show how efficiently the engine produces thrust. It is defined as

$$\frac{\text{Uninstalled thrust}}{\text{Fuel weight flow rate}} = I_{sp} = \frac{F}{g_0 \dot{m}_f} \quad (3.47)$$

3.4.1.4 Propulsive Efficiency

The propulsive efficiency is the ratio of thrust power to engine mechanical power. It can be defined as

$$\eta_p = \frac{2\left\{(1+f)\frac{V_e}{V_0} - 1\right\}}{\left\{(1+f)\left(\frac{V_e}{V_0}\right)^2 - 1\right\}} \quad (3.48)$$

Nevertheless, by following Equation 3.48 the propulsive efficiency can actually exceed 1. This happens when the fuel/air ratio is large enough. Therefore, a more logical equation can be defined, neglecting the fuel/air ratio. This equation follows below.

$$\eta_p = \frac{2}{\frac{V_e}{V_0} + 1} \quad (3.49)$$

3.4.1.5 Thermal Efficiency

Thermal efficiency is the ratio of engine mechanical power to chemical energy rate. It is defined as

$$\eta_{th} = \frac{(1+f)\frac{V_e^2}{2} - \frac{V_0^2}{2}}{fh_{PR}} \quad (3.50)$$

3.4.1.6 Overall Efficiency

The overall efficiency demonstrates "how well the engine uses the energy originally deposited in the fuel tanks" [4]. It is defined as

$$\text{Overall efficiency } = \eta_o = \frac{\text{Thrust power}}{\text{Chemical energy rate}} = \frac{FV_0}{\dot{m}_f h_{PR}} \quad (3.51)$$

The overall efficiency can also be easily calculated by the product of both the thermal and propulsive efficiency, as defined by

$$\eta_o = \eta_{th} \cdot \eta_p \quad (3.52)$$

3.4.2 High-Level Flowchart

Having described the methodology implemented, a high-level flowchart of the developed tool follows in Figure 3.4. Additionally, the Python code follows attached to this dissertation in Annex A.2.

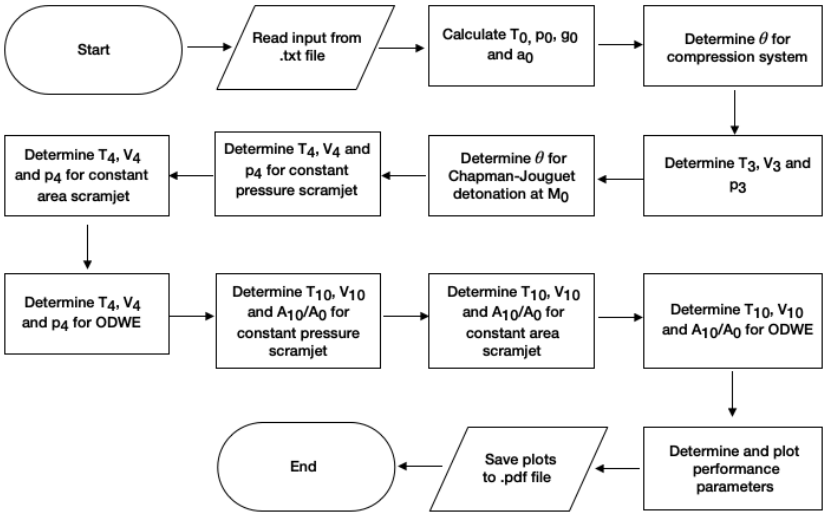

Figure 3.4: High-level flowchart of the developed tool.

Chapter 4

Results

4.1 Model Validation

Before implementing a case study, running the tool and analysing the results, it is important to run some tests and compare the results obtained by the tool and those available in the open literature. This will allow a better understanding of the accuracy of the model implemented, know its limitations, and also contribute to greater confidence in the final results and conclusions.

4.1.1 Compression System

Firstly, the compression system model implemented is tested for on-design conditions. Apart from the operating conditions, the code receives as input the desired T_{ratio}. It then finds the wedge angle, which is the same for all shocks, that assures that specific T_{ratio} at the end of the compression system. Only weak shocks are considered to assure supersonic flow throughout the engine. A series of four oblique shock waves is considered, as already discussed in 3.2.2. The input of the validation test follows below.

Table 4.1: Input data for compression system validation.

Property	Assigned Value
M_0	10
T_0	$288.15\ K$
T_{ratio}	2
γ_c	1.362

The results of the validation test follow in Table 4.2.

Table 4.2: Results of the compression system validation test.

Wedge Angle [°]	$T_3\ [K]$	T_{ratio}	Error [%]
3.177	575.7	1.998	0.1019

The tool developed finds the wedge angle by iteration until the difference between the desired T_{ratio} and the actual T_{ratio} calculated by the tool is less than 0.01. For greater accuracy, this can be easily changed by decreasing this difference. Nevertheless, that will increase the time needed for computation. As the error is less than 1%, the chosen interval is considered to be a great compromise between accuracy and computational time.

4.1.2 Scramjet

To validate the mathematical model implemented for the scramjet engine, results obtained by the developed tool were compared with those from Heiser and Pratt [4]. Table 4.3 shows the input data that was used for model validation.

Table 4.3: Input data for model validation [4].

Property	Assigned Value
T_0	$222\,K$
V_0	$3048\,m/s$
T_3	$1556\,K$
V_3	$2530\,m/s$
η_b	0.9
η_e	0.9
f	0.04
$\frac{V_{fx}}{V_3}$	0.5
$\frac{V_f}{V_3}$	0.5
$C_f \frac{A_w}{A_3}$	0.1
C_{pb}	$1.51\,kJ/kgK$
C_{pe}	$1.51\,kJ/kgK$
fh_{PR}	$3510\,kJ/kg$
h_f	0
T^o	$222\,K$
γ_b	1.238
γ_e	1.238
R	$289.3\,(m/s)^2/K$
$\frac{p_4}{p_0}$	258
$\frac{p_{10}}{p_0}$	1.4

Tables 4.4 and 4.5 present the results from Heiser and Pratt [4] for the scramjet engine with both constant pressure and constant area combustion. In addition, it also presents the results obtained with the tool developed and the relative error for each property.

Table 4.4: Comparison of constant pressure scramjet results obtained by the tool developed and Heiser et al. [4].

Property	Constant Pressure [4]	Constant Pressure	Error [%]
T_4	$3740\,K$	$3730.86\,K$	0.2444
V_4	$2360\,m/s$	$2359.71\,m/s$	0.01222
T_{10}	$1610\,K$	$1609.05\,K$	0.05881
V_{10}	$3460\,m/s$	$3460.65\,m/s$	0.01875
$\frac{F}{\dot{m}_0}$	$590\,Ns/kg$	$591.09\,Ns/kg$	0.1848
η_{th}	0.450	0.4508	0.1845
I_{sp}	$1504\,s$	$1506.86\,s$	0.1902

Looking into the relative error column of Table 4.4, one can conclude that no property possesses a relative error above 1%. This small error is likely to be explained by the rounding of the results presented by Heiser and Pratt. Therefore, the mathematical model for the constant pressure scramjet is validated.

Looking into the relative error column of Table 4.5, it can once again be concluded that

Table 4.5: Comparison of constant area scramjet results obtained by the tool developed and Heiser et al. [4].

Property	Constant Area [4]	Constant Area	Error [%]
T_4	$4500\,K$	$4480.67\,K$	0.4296
V_4	$1810\,m/s$	$1817.63\,m/s$	0.4221
$\frac{p_4}{p_0}$	1080	1075.47	0.4193
T_{10}	$1580\,K$	$1577.24\,K$	0.1748
V_{10}	$3470\,m/s$	$3474.50\,m/s$	0.1298
$\frac{F}{\dot{m}_0}$	$603\,Ns/kg$	$604.71\,Ns/kg$	0.2844
η_{th}	0.464	0.4651	0.2295
I_{sp}	$1538\,s$	$1541.59\,s$	0.2336

no property possesses a relative error above 1%. This small error is likely to be explained by the rounding of the results presented by Heiser and Pratt. That being said, the mathematical model for the constant area scramjet is assumed to be valid.

4.1.3 Oblique Detonation Wave Engine

To validate the mathematical model for the ODWE, results obtained by the developed tool were compared with those from Heiser and Pratt [4]. Using an online tool, data points from the Chapman-Jouguet locus (blue curve) on Figure 4.1 from [4] were extracted. Making use of the program developed for this dissertation, the very same curve was obtained. The comparison follows in Figure 4.2.

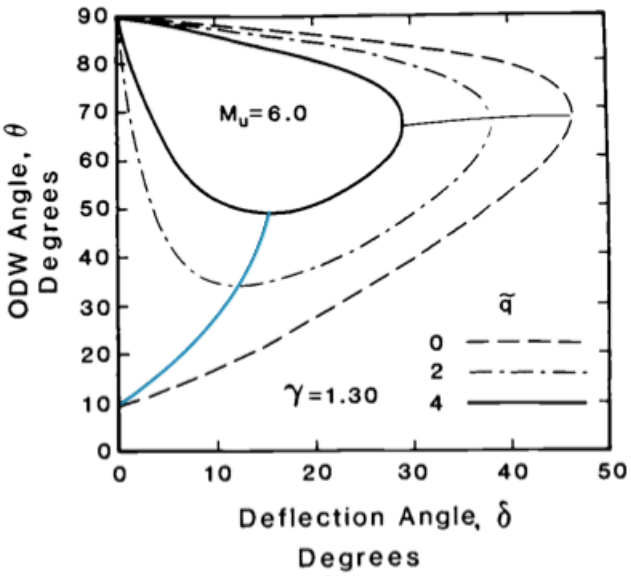

Figure 4.1: Oblique detonation wave angle as a function of deflection angle and heat addition, for constant upstream conditions and an upstream Mach number of 6 [4].

It can be seen that the curves are almost overlapping each other. Nevertheless, from a deflection angle of around $6°$, there is a small gap between both curves. This is considered acceptable as the tool used to extract the data points is not 100% accurate.

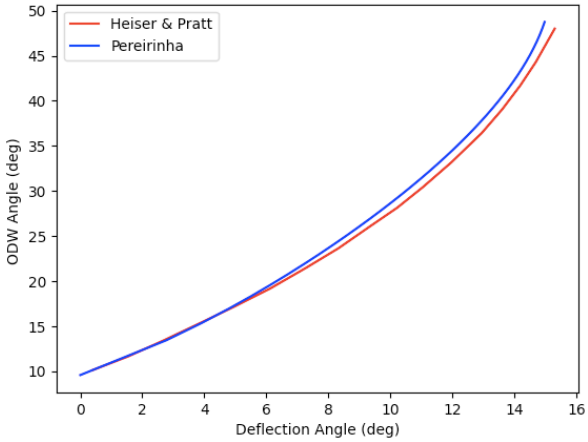

Figure 4.2: Comparison of Chapman-Jouguet locus obtained by the tool developed and Heiser et al. [4].

In order to further validate the model, the NASA Computer programme CEA (Chemical Equilibrium with Applications) was also used to simulate and determine properties after a Chapman-Jouguet detonation. The results obtained from CEA were then compared to those obtained by the tool developed. For the test, the oxidizer selected was air and the fuel was hydrogen. The input used for this validation test follows in Table 4.6.

Table 4.6: Input data for model validation.

Property	Assigned Value
T_0	$298\,K$
p_0	$101325\,Pa$
ϕ	1
M_{CJ}	4.8335
a_{CJ}	$406.6\,m/s$
ρ_{ratio}	1.8042
γ_0	1.4015

The output obtained from the NASA CEA and the tool developed follows in Table 4.7. The relative error was also calculated in order to better understand the degree of accuracy of the results produced.

Table 4.7: Comparison of results obtained by NASA CEA and the tool developed.

Property	NASA CEA	Pereirinha	Error [%]
p_{ratio}	15.595	15.594	0.005385
T_{ratio}	9.878	9.923	0.4569

Once again, the relative error falls under 1% which validates the mathematical model implemented to calculate both temperature and pressure after a Chapman-Jouget detonation. At this point, the model is assumed to be validated and with great accuracy, when compared to the data from Heiser and Pratt [4] and the results from NASA CEA.

4.2 Parametric Studies

To create the code, several functions were defined in order to make it more understandable to others. Additionally, this allows using some lines of code multiple times, instead of having to rewrite them. These are also helpful to study certain parts of the engine independently and perform parametric studies to have a better understanding of how some parameters influence others. Additionally, results from these studies will also be helpful when choosing the input data for the case study.

4.2.1 Compression System

Firstly, the compression system will be studied. It is of interest to understand how the T_{ratio} affects both the η_{KE} and η_c for several M_0, considering four oblique shock waves. This can be seen in Figure 4.3.

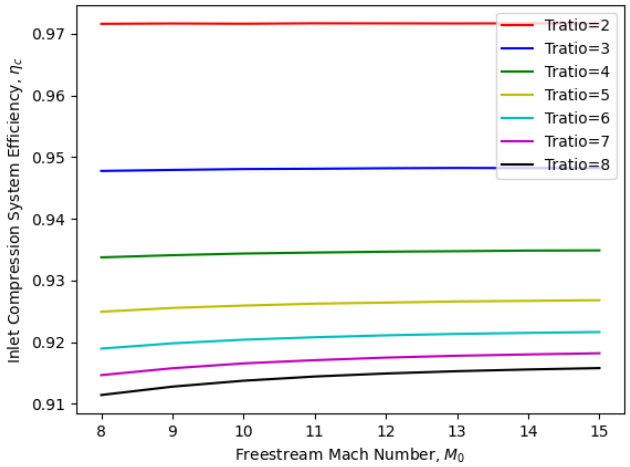

Figure 4.3: Inlet compression system efficiency as a function of M_0 for several T_{ratio}, $\gamma_c = 1.362$.

It can be concluded that as the T_{ratio} increases, for the same M_0, the inlet compression system efficiency decreases. The results here presented can also be validated by taking into account Figure 3.3. On the other hand, in Figure 4.4 it can be seen how the kinetic energy efficiency varies with both M_0 and T_{ratio}.

It can be concluded that increasing the T_{ratio} also has a negative impact on the kinetic energy efficiency. Taking this into consideration, when choosing the desired T_{ratio} to design the inlet of a hypersonic airbreathing engine, the negative influence of T_{ratio} on both efficiencies should be taken into account. Nevertheless, a low T_{ratio} impacts negatively the overall performance of the engine, so a trade-off study should be performed.

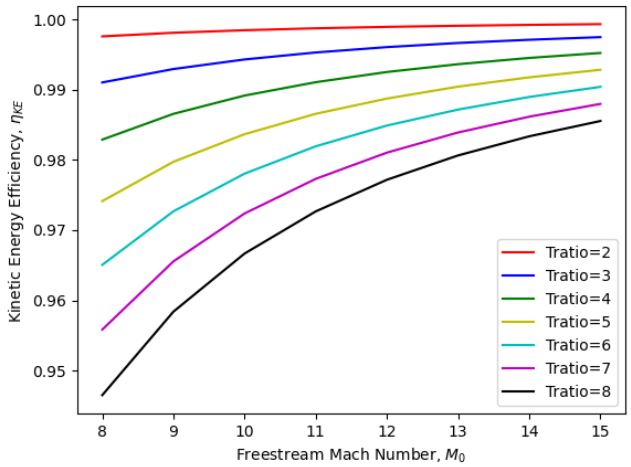

Figure 4.4: Kinetic energy efficiency as a function of M_0 for several T_{ratio}, $\gamma_c = 1.362$.

In Figure 4.5, it can be seen how the burner entry Mach number, M_3, varies with the freestream Mach number, M_0, for different values of T_{ratio}. The higher the T_{ratio}, the lower M_3 is. This graph is mainly helpful to assure that the T_{ratio} chosen allows for a supersonic burner entry Mach number, so supersonic combustion can happen. It is also worth mentioning that a low M_3 can be advantageous, as it can minimise some of the difficulties associated with supersonic combustion, such as fuel/air mixing [26]. On the other hand, it can be seen that a low M_3 means a high T_{ratio}. This leads to high temperatures inside the engine, causing high thermal stress and requiring special materials that can withstand such stresses.

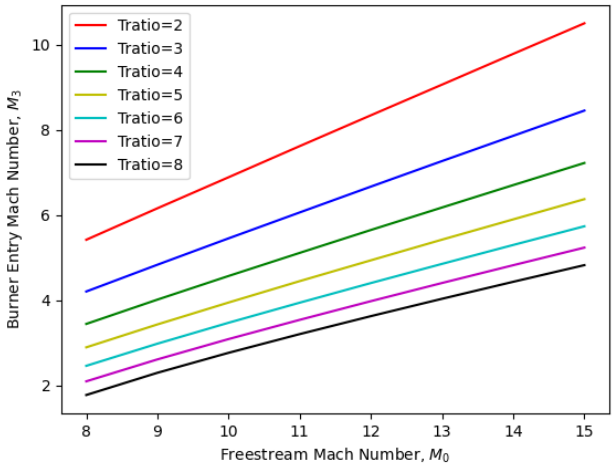

Figure 4.5: Burner entry Mach number, M_3, as a function of M_0 for several T_{ratio}, $\gamma_c = 1.362$.

4.2.2 Oblique Detonation Wave

Oblique detonation waves (ODWs) were also studied and subjected to parametric studies. To better understand the influence $\tilde{Q}$ has on the necessary wedge angle to generate a Chapman-Jouguet detonation, Figure 4.6 was plotted.

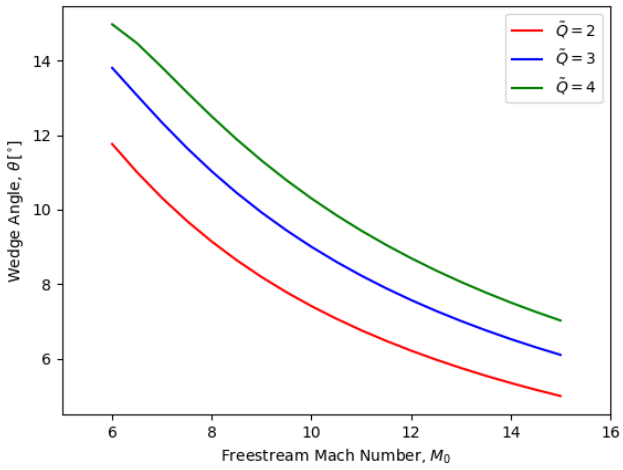

Figure 4.6: Wedge angle as a function of freestream Mach number for $\tilde{Q} = 2$, $\tilde{Q} = 3$, $\tilde{Q} = 4$ and $\gamma_c = 1.362$.

On the other hand, to better understand the influence $\tilde{Q}$ has on the detonation angle of a Chapman-Jouguet detonation, Figure 4.7 was plotted.

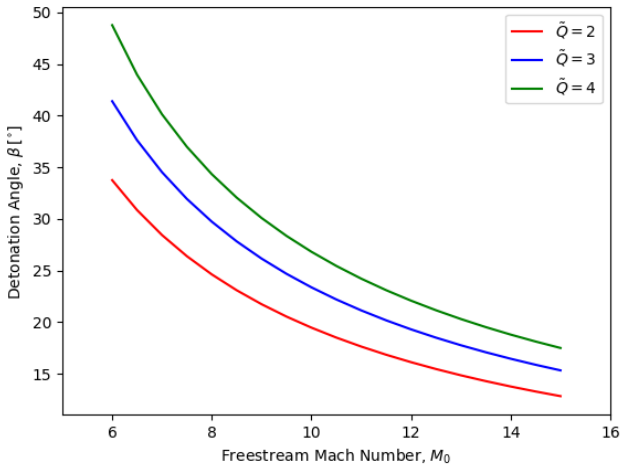

Figure 4.7: Detonation angle as a function of freestream Mach number for $\tilde{Q} = 2$, $\tilde{Q} = 3$, $\tilde{Q} = 4$ and $\gamma_c = 1.362$.

By increasing $\tilde{Q}$, a higher wedge angle is necessary to generate a Chapman-Jouguet detonation, which logically leads to a higher detonation angle. These plots are also helpful in case the wedge angle can be varied in flight to generate a Chapman-Jouguet detonation for all M_0.

Afterwards, it was studied how the detonation pressure and temperature ratio are affected by the dimensionless ODW heat flux, $\tilde{Q}$. For this, η_b was considered 1. Figures 4.8 and 4.9 were plotted for the following conditions upstream of the detonation: $p = 101325\,Pa$, $T = 298\,K$, $\gamma = 1.4$ and $C_p = 1005\,J/kgK$.

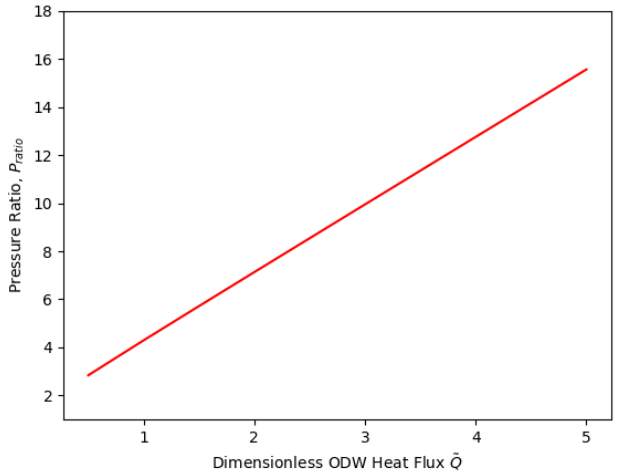

Figure 4.8: Pressure ratio as a function of dimensionless ODW heat flux.

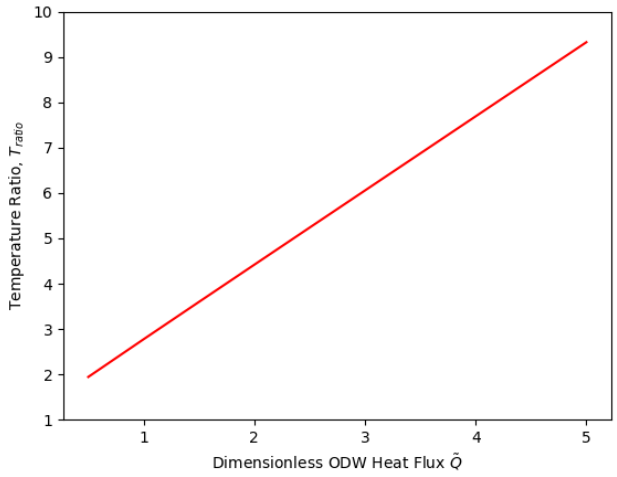

Figure 4.9: Temperature ratio as a function of dimensionless ODW heat flux.

For the range considered, it can be concluded that as the dimensionless ODW heat flux increases, both T_{ratio} and p_{ratio} increase in an approximately linear manner.

4.2.3 Scramjet Combustion

In this section, the influence of ϕ is studied for both constant pressure and constant area burner. In Table 4.8, properties used for this study are specified.

Table 4.8: Input for the study of influence of ϕ.

Property	Assigned Value
On-Design M_0	8
On-Design T_{ratio}	2
$\frac{V_{fx}}{V_3}$	0.5
$\frac{V_f}{V_3}$	0.5
$C_f \frac{A_w}{A_3}$	0
C_{pb}	$1510\ J/kgK$
T^o	$222\ K$
h_{PR}	$119.96\ MJ/kg$
η_b	1

The study is performed considering a lean, stoichiometric and rich mixture of H_2/air, $\phi = 0.5$, $\phi = 1$ and $\phi = 1.5$, respectively.

4.2.3.1 Constant Pressure Burner

For the constant pressure burner, results follow in Figures 4.10, 4.11 and 4.12. As expected, increasing the equivalence ratio leads to higher temperatures at the burner exit. As an example, by doubling ϕ from 0.5 to 1, at $M_0 = 8$, there is an approximate increase of 65 $\%$ in the temperature at the burner exit.

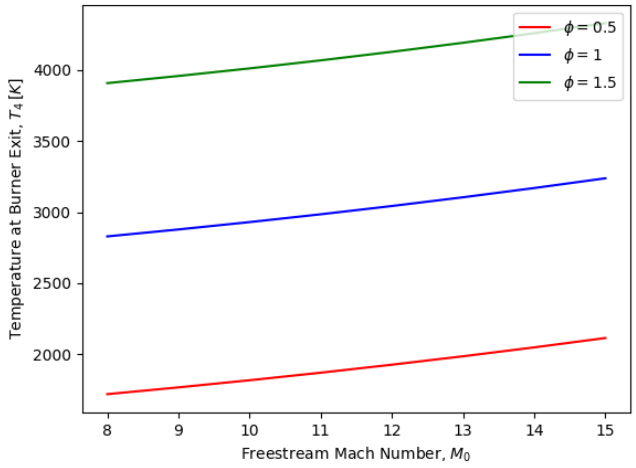

Figure 4.10: Temperature at burner exit as a function of M_0 for $\phi = 0.5$, $\phi = 1$ and $\phi = 1.5$.

On the other hand, the lower ϕ is, the higher is V_4. Nevertheless, as this is the case of a constant pressure burner, velocity changes only slightly with ϕ, very little when compared with how T_4 changes with ϕ.

In a constant pressure burner, the area across the burner needs to increase, so pressure can be maintained. In Figure 4.12, it can be seen that increasing ϕ also leads to a higher variation of cross-section area across the burner. For the overall engine this can mean

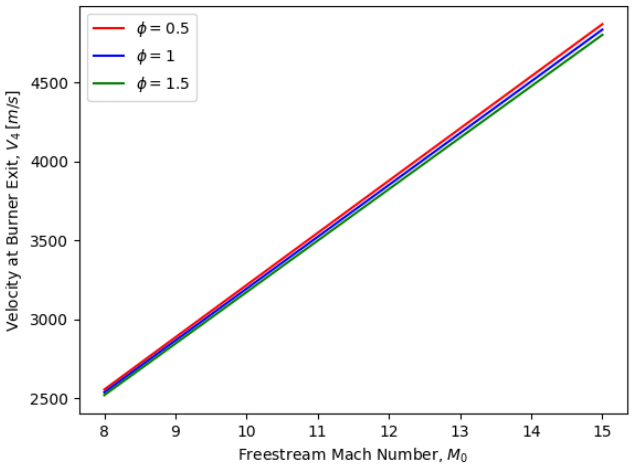

Figure 4.11: Velocity at burner exit as a function of M_0 for $\phi = 0.5$, $\phi = 1$ and $\phi = 1.5$.

high penalties, as by increasing the cross-section, the drag created will also increase.

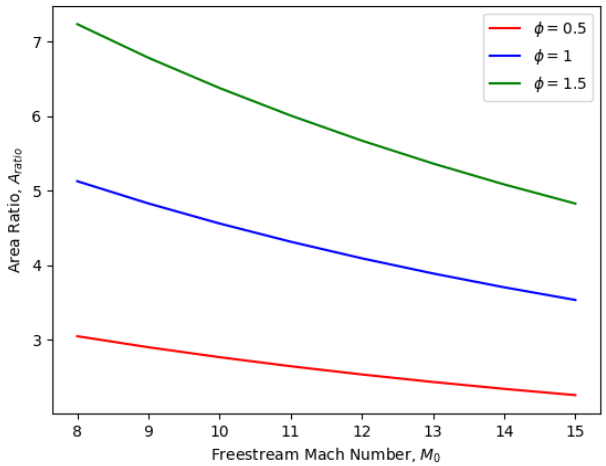

Figure 4.12: Area ratio as a function of M_0 for $\phi = 0.5$, $\phi = 1$ and $\phi = 1.5$.

4.2.3.2 Constant Area Burner

Similarly of what was done for the constant pressure burner, for the constant area burner, results follow in Figures 4.13, 4.14 and 4.15. Additionally, in these conditions, by comparing the results for the constant area and constant pressure burner, it can be seen that the temperature at the burner exit is higher for the constant area. Also, just like it was mentioned for the constant pressure burner case, doubling ϕ from 0.5 to 1 at $M_0 = 8$ leads to an increase in T_4 of approximately $72\,\%$.

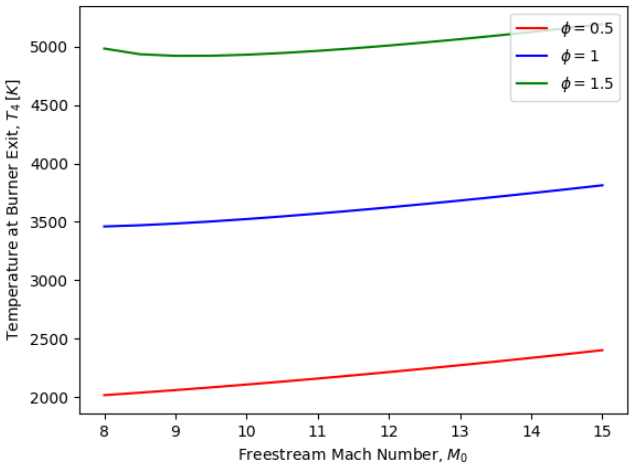

Figure 4.13: Temperature ratio as a function of M_0 for $\phi = 0.5$, $\phi = 1$ and $\phi = 1.5$.

Looking into Figure 4.14, it can be seen how much pressure increases through the engine until the burner exit. The goal of the plot was to verify that the equivalence ratio increases this pressure ratio, which is indeed verified.

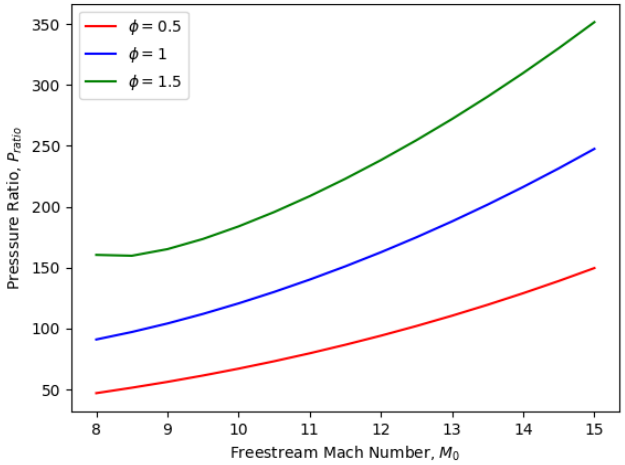

Figure 4.14: Freestream to burner exit pressure ratio as a function of M_0 for $\phi = 0.5$, $\phi = 1$ and $\phi = 1.5$.

Lastly, once again it is concluded that the equivalence ratio does not influence V_4, as much as it influences both T_4 and p_{ratio}. Additionally, V_4 increases with M_0 and also with the decrease of ϕ. When deciding on the equivalence ratio, the variation of all of these parameters should be studied in order to decide which ϕ suits the needs of the mission the most. As for the case study to be addressed in the following section, ϕ will be considered 1.

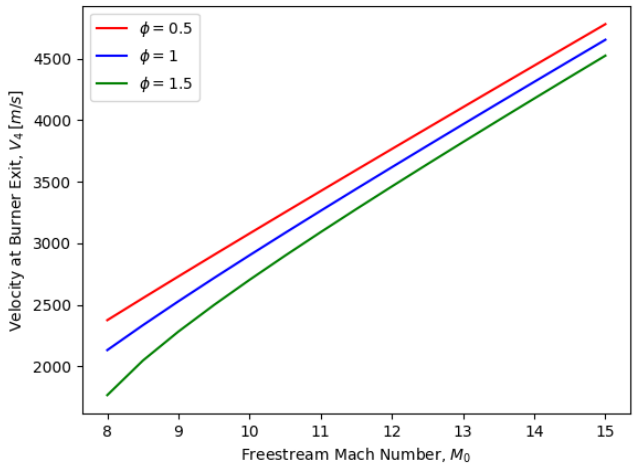

Figure 4.15: Velocity at burner exit as a function of M_0 for $\phi = 0.5$, $\phi = 1$ and $\phi = 1.5$.

4.3 Case Study

Having performed a series of parametric studies and with the insights taken from its results, a case study was created. This case study ultimately fulfils the end goal of this dissertation, which is to compare the performance of a scramjet engine with an ODWE.

Some simplifications have been introduced, as not introducing them would lead to complex methods that go far beyond the scope and aim of this dissertation. This means that attention should be paid when assigning certain constants its value, such as γ and C_p. As one can easily deduce, the input data chosen highly influences the results produced. For this project, the input data was carefully chosen in order to be as accurate and realistic as possible.

4.3.1 Input Data

The input data for this case study follows below in Table 4.9. Furthermore, it is listed in the same order as the input file of the programme. It should be kept in mind that the lowest Mach number possible to be analysed is $M_0 = 8$, as no isolator was taken into account while developing this project. As for the range of Mach numbers to be analysed, it is advisable for it to be small, as some properties are taken as constant throughout the range. Another property that requires attention when choosing its value is the T_{ratio} for compression system design. The reason behind this is that preignition should be avoided. As mentioned in section 3.3.2, the temperature upstream of the detonation should be kept

below $1000\,K$ to prevent preignition from occurring. If this is not met, the code will print a warning, asking the user to reduce the T_{ratio}. In order to meet this requirement for all the Mach numbers considered, whilst not penalising performance, the T_{ratio} chosen is 2.

Table 4.9: Case study input.

Property	Assigned value
$h\,[m]$	0
M_{OD}	10
$M_{upper\,bound}$	15
T_{ratio}	2
γ_c	1.362
Scramjet γ_b	1.238
ODWE γ_b	1.170
Scramjet γ_e	1.238
ODWE γ_e	1.170
$C_{p0}\,[J/kgK]$	1005
$C_{pc}\,[J/kgK]$	1090
Scramjet $C_{pb}\,[J/kgK]$	1510
ODWE $C_{pb}\,[J/kgK]$	2000
Scramjet $C_{pe}\,[J/kgK]$	1510
ODWE $C_{pe}\,[J/kgK]$	2000
$\frac{V_{fx}}{V_3}$	0.5
$\frac{V_f}{V_3}$	0.5
Scramjet η_b	0.9
ODWE η_b	0.9
Scramjet η_e	0.9
ODWE η_e	0.9
x of CxHy	0
y of CxHy	2
$h_{PR}\,[MJ/kg]$	119.96

Scramjet related properties, such as γ_b, γ_e, C_{pb} and C_{pe} were taken from Heiser et al. [4]. Additionally, $\frac{V_{fx}}{V_3}$ and $\frac{V_f}{V_3}$ were also taken from the very same source, as well as γ_c, which is the same for both the scramjets and the ODWE. Nevertheless, it would not be correct to take for the ODWE γ_b, γ_e, C_{pb} and C_{pe} the same as the scramjet engine. This is because, in the burner, the temperature and pressure are much higher in the ODWE than in the scramjet engine. Thus, some research was conducted in order to assign these parameters a realistic value. As such, the properties after the detonation for $M_0 = 10$ were investigated and it was concluded that T_4 was approximately $5000\,K$. At these high temperatures, both C_p and γ vary more substantially with temperature than with pressure, therefore, the influence of pressure is neglected here and only the influence of temperature is taken into account. Also, considering the composition of the mixture after combustion, it was decided to set $C_{pb} = C_{pe} = 2000 J/kgK$ and $\gamma_b = \gamma_e = 1.170$. As for the efficiencies, they were all assumed as 0.9 [4].

4.3.2 Performance Comparison

Firstly, specific thrust as a function of freestream Mach number was plotted, Figure 4.16. As expected, maximum specific thrust is achieved at design Mach number, $M_0 = 10$, and decays as the Mach number increases for all three engines. As for the scramjet engines, constant area combustion has a higher specific thrust than the constant pressure combustion scramjet. Nevertheless, the ODWE offers a much higher specific thrust than the scramjet engine. On the other hand, the curve of the ODWE has a higher slope, meaning that for the case study here analysed, the ODWE is more affected by off-design operation than the other engines.

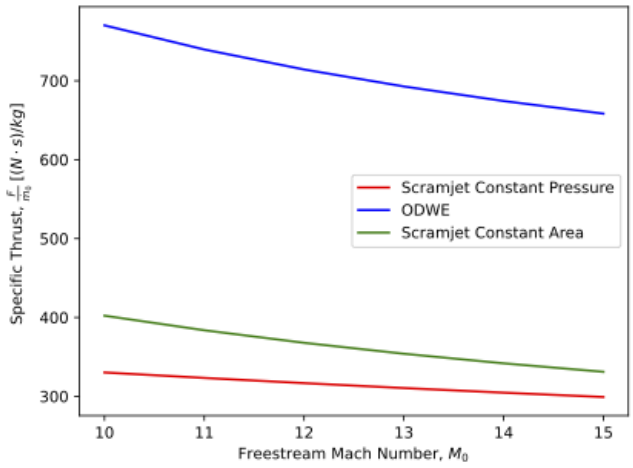

Figure 4.16: Specific thrust as a function of freestream Mach number for the three engines studied.

Taking into consideration these results, and Equation 3.46 one can expect the engine that produces the highest specific thrust to have the lowest specific fuel consumption. Figure 4.17 shows exactly that. Additionally, as expected, the lower specific fuel consumption is verified at the design Mach number, increasing as the freestream Mach number increases. Then, in Figure 4.18 one of the most important performance parameters is plotted, the specific impulse. As Vanyai et al. [22] mentioned in their work, constant area scramjet usually produces the highest specific impulse for the same burner entry conditions, when compared to other scramjet combustion processes. The results of this project show exactly that, meaning the conclusions taken here are in accordance with those present in current literature. As for the ODWE, it performs better than both scramjet engines. For reference, for this case study and $M_0 = 10$, the I_{sp} produced by the ODWE is approximately 1.91 times higher than that of the constant area scramjet, and 2.33 times for the constant pressure scramjet.

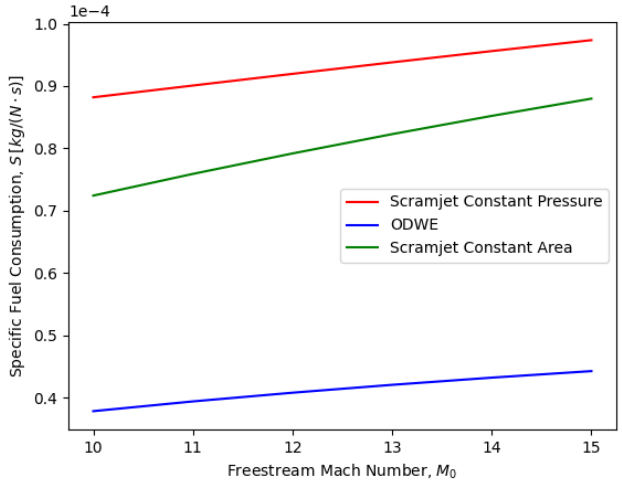

Figure 4.17: Specific fuel consumption as a function of freestream Mach number for the three engines studied.

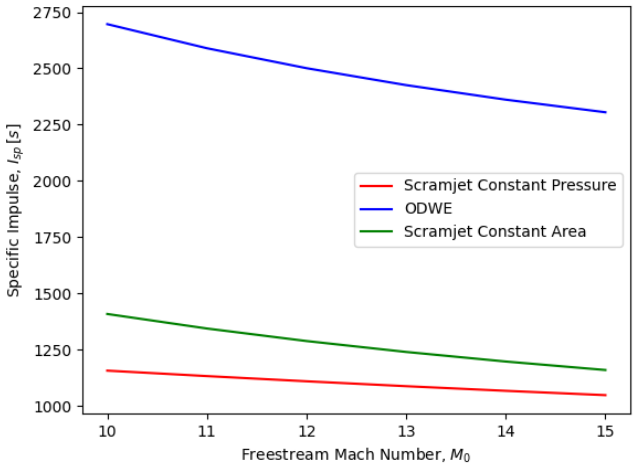

Figure 4.18: Specific impulse as a function of freestream Mach number for the three engines studied.

Regarding the propulsive efficiency, results follow in Figure 4.19. Compared to the other engines, the ODWE has the lowest propulsive efficiency as it has the highest exhaust velocity, V_e. On the other hand, $\frac{V_e}{V_0}$ is the lowest for the constant pressure scramjet, which explains why this engine has the highest propulsive efficiency. A key point to retain from this analysis is that considering the 3 engines subjected to this study, the constant pressure scramjet is the one that converts engine mechanical power into thrust power more efficiently.

As for the thermal efficiency, looking into Figure 4.20, it can be concluded that the ODWE indeed has a much higher thermal efficiency than the scramjet engines. This result is also in accordance with Jiang et al. [14], which suggests that the ODWE is a promising engine configuration regarding thermal efficiency. Concerning scramjet engines, the con-

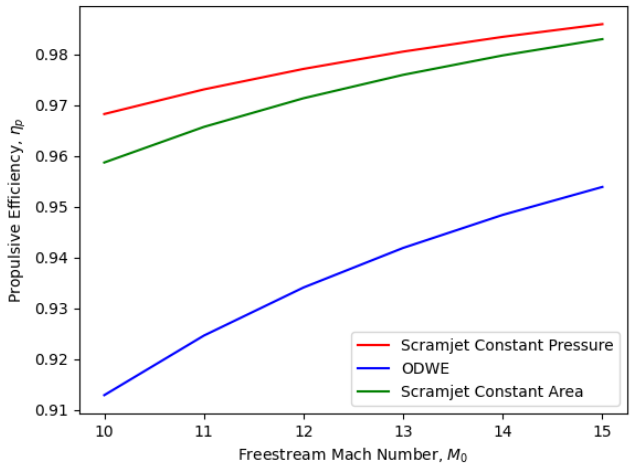

Figure 4.19: Propulsive efficiency as a function of freestream Mach number for the three engines studied.

stant area combustion has higher thermal efficiency, meaning the constant area process is more efficient in converting chemical energy rate into engine mechanical power than the constant pressure process.

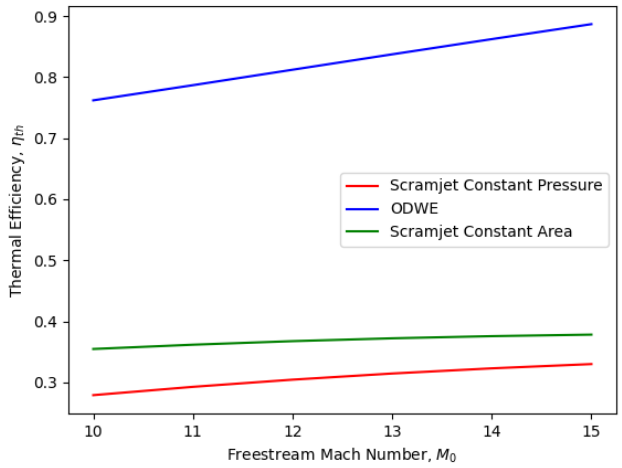

Figure 4.20: Thermal efficiency as a function of freestream Mach number for the three engines studied.

In Figure 4.21, the overall efficiency is plotted. This performance parameter shows how efficiently the engine uses the energy that was initially stored in the fuel tanks or, alternatively, how much fuel must be carried in order to supply the required amount of energy for a certain mission. Therefore, it can be concluded that once again the ODWE is the most efficient engine, followed by the constant area scramjet, and then the constant pressure scramjet.

All the plots above fulfil the goal of this project, which was to compare the performance

of the three engines. Having analysed them, it can firmly be concluded that the ODWE is a promising engine configuration with outstanding performance when compared to both scramjet engines here analysed. Additionally, this study also allows us to better understand the difference in performance between the two scramjet combustion processes. Thus, it can be concluded that the constant area combustion scramjet performs better than the constant pressure process.

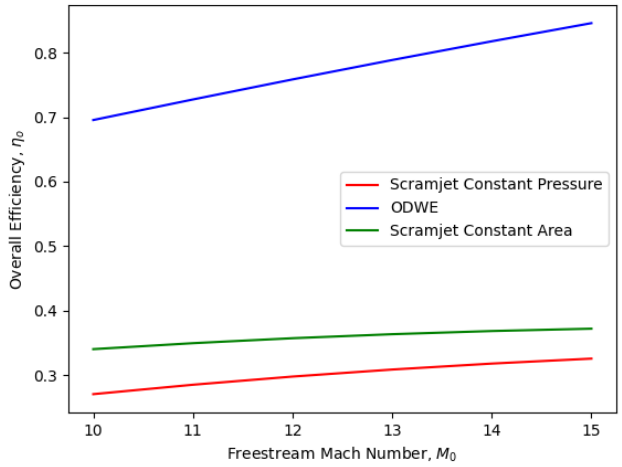

Figure 4.21: Overall efficiency as a function of freestream Mach number for the three engines studied.

Last but not least, it was decided to plot $\frac{A_{10}}{A_0}$. Although it is not a performance parameter, it is considered very important as it is an indicator of how much drag the engine geometry will create. Also, if variable nozzle geometry is considered, then Figure 4.22 shows how A_{10} should change over the considered Mach range, for constant A_0.

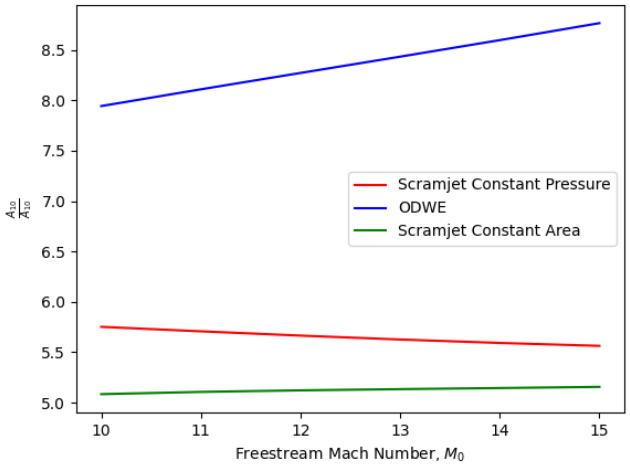

Figure 4.22: A_{ratio} as a function of freestream Mach number for the three engines studied.

Chapter 5

Conclusion

5.1 Summary

The main goal of this thesis was to compare the performance of the ODWE with the performance of scramjet engines. With that aim, a tool was created in Python. This project falls well within all the research conducted to investigate new engine configurations that can potentially replace scramjets for hypersonic speeds. Given the advantages hypersonic airbreathing propulsion can offer when compared to rockets for launching payloads into space, or when compared to conventional engines for commercial flights, this is a field worth studying.

Firstly, research was conducted to define the mathematical model to be implemented. It was decided to do a one-dimensional study, as the aim of the project is performance comparison for early-stage engine development, and not meticulous engine design. From all the one-dimensional methods, the stream thrust analysis was chosen for the scramjet engine, as this approach is very often mentioned in the open literature as the most accurate. To model the detonation process of the ODWE, the work of Pratt et al. [11] was followed, but η_b was also included in order to make sure the analysis of the scramjet engine and the ODWE include the same parameters. Additionally, for each engine station, it was decided to assign C_p and γ values in accordance with the expected conditions in that station. Furthermore, these are also constant over the range of Mach numbers analysed. This simplifies the analysis greatly and without substantially compromising the accuracy of the results, especially if a small range of Mach numbers is studied.

To assure the results obtained were valid, some tests were run and compared with results found in the open literature. For the scramjet engine, both constant area and constant pressure combustion, the results were compared with those present in Heiser et al. [4]. The overall result of the model validation for the scramjet engine was considered successful, as the relative error of all properties was well below 1%. As for the ODWE, the results were once again compared with those from Heiser et al. [4], but also with NASA Com-

puter programme CEA (Chemical Equilibrium with Applications). Heiser et al. [4] was used to validate the Chapman-Jouguet locus obtained for an upstream Mach number of 6. On the other hand, the results obtained from a case study run at NASA CEA were used to validate the functions developed in the code that calculate properties downstream of the detonation. Once again, the relative error fell well below 1%, so the tool is assumed valid.

Besides performance comparison, it was also decided to perform some parametric studies with the functions developed and implemented in the programme. The goal of this study was to better understand the influence some parameters have on the engine, but also to have some criteria when choosing the input data for the case study that ultimately fulfils the goal of this dissertation.

Lastly, the case study was created and its results analysed. It was concluded that indeed the ODWE performs very well when compared with the scramjet engine. The difference in performance is solely due to the combustion mode, as the rest of the engine stations are analysed using the same mathematical model. As it was verified, for $M_0 = 10$, the ODWE has a specific impulse of 1.91 and 2.33 times higher than the scramjet engine, constant area and constant pressure respectively. Furthermore, the ODWE also has the lowest specific fuel consumption and is a great alternative to achieving high thermal efficiency, which is an issue for scramjet engines. In addition, this study also allowed to understand which combustion process performs the best. The constant area scramjet outperformed the constant pressure in all the performance parameters studied. Nevertheless, the constant pressure process is usually chosen because it avoids the need to build the structure primarily to withstand the peak pressure, and avoids the potential of boundary-layer separation, [4]. Similarly, even though the ODWE outperforms both scramjets, there are still many obstacles in the way of this technology, such as the stability of the ODW and also materials that can withstand such conditions after the detonation.

To conclude, the goal of this project was accomplished and validates the growing interest in the ODWE for hypersonic flight. Additionally, it also solidifies the use of detonations for propulsion applications.

5.2 Future Work

Concerning future works, some improvements could be implemented to the code, in order to generate more realistic results and to allow for a broader analysis of the engines. As an example, more scramjet combustion processes could be studied, such as constant volume or constant velocity. In addition to this, engine geometry could also be incorporated into the programme, in order to estimate the dimensions of each station, and the overall engine as well. This would allow for a very complete analysis that can be very valuable in early-stage engine development.

Bibliography

[1] R. Dunlap, R. L. Brehm, and J. A. Nicholls, "A preliminary study of the application of steady-state detonative combustion to a reaction engine," *Journal of Jet Propulsion*, vol. 28, pp. 451–456, 7 1958. 3, 5, 6

[2] S. A. Ashford and G. Emanuel, "Oblique detonation wave engine performance prediction," *Journal of Propulsion and Power*, vol. 12, pp. 322–327, 1996. 3, 6, 19

[3] Z. Jiang, Z. Zhang, Y. Liu, C. Wang, and C. Luo, "Criteria for hypersonic airbreathing propulsion and its experimental verification," *Chinese Journal of Aeronautics*, vol. 34, pp. 94–104, 3 2021. 3, 6

[4] W. H. Heiser and D. T. Pratt, *Hypersonic airbreathing propulsion*. American Institute of Aeronautics and Astronautics, 1994. 4, 8, 13, 14, 15, 16, 17, 18, 20, 21, 22, 24, 26, 27, 28, 37, 43, 44

[5] K. N. Roberts, "Analysis and design of a hypersonic scramjet engine with a starting mach number of 4.00," Master's thesis, The University of Texas at Arlington, August 2008. 4, 14, 21

[6] Y. Tsujikawa, Y. Tsukamoto, and S. Fujii, "Performance analysis of scramjet engine with quasi-one-dimensional flow model," *International Journal of Hydrogen Energy*, vol. 16, pp. 135–142, 1 1991. 4

[7] T. C. Rolim and F. K. Lu, "Design and stream thrust analysis of a scramjet engine for acceleration mission from 2 to 3 km/s," *51st AIAA Aerospace Sciences Meeting including the New Horizons Forum and Aerospace Exposition 2013*, 2013. 4, 17

[8] K. Tran, "One dimensional analysis program for scramjet and ramjet flowpaths," Master's thesis, Virginia Polytechnic Institute and State University, Blacksburg, 2010. 4

[9] P. M. Diéguez, J. López-San Martín, I. Idareta, I. Uriz, G. Arzamendi, and L. M. Gandía, "Chapter 18 - hydrogen hazards and risks analysis through cfd simulations," in *Renewable Hydrogen Technologies*, L. M. Gandía, G. Arzamendi, and P. M. Diéguez, Eds. Amsterdam: Elsevier, 2013, pp. 437–452. [Online]. Available: https://www.sciencedirect.com/science/article/pii/B9780444563521000180 5

[10] J. H. S. Lee, *The Detonation Phenomenon*. Cambridge University Press, 2008. 5, 10

[11] D. T. Pratt, J. W. Humphrey, and D. E. Glenn, "Morphology of standing oblique detonation waves," *Journal of Propulsion and Power*, vol. 7, pp. 837–845, 1991. 5, 6, 9, 20, 43

[12] R. M, "Propulsion par statoreacteur a detonation," *ComptesRendus de Acad. ScL de Paris*, vol. 222, Feb 1, 1946. 5

[13] K. Iwata, S. Nakaya, and M. Tsue, "Numerical simulation of incompletely premixed oblique detonation stabilized on a solid surface," *Transactions of The Japan Society for Aeronautical and Space Sciences, Space Technology Japan*, vol. 14, 2016. 6

[14] Z. Zhang, C. Wen, W. Zhang, Y. Liu, and Z. Jiang, "Formation of stabilized oblique detonation waves in a combustor," *Combustion and Flame*, vol. 223, pp. 423–436, 1 2021. 5, 39

[15] M. Valorani, M. D. Giacinto, and C. Buongiorno, "Performance prediction for oblique detonation wave engines (odwe) †," pp. 211–228, 2001. [Online]. Available: www.elsevier.com/locate/actaastro 5

[16] D. A. Rosato, M. Thornton, J. Sosa, C. Bachman, G. B. Goodwin, and K. A. Ahmed, "Stabilized detonation for hypersonic propulsion," *Proceedings of the National Academy of Sciences*, vol. 118, no. 20, p. e2102244118, 2021. [Online]. Available: https://www.pnas.org/doi/abs/10.1073/pnas.2102244118 6

[17] J. L. Cambier, H. Adelman, and G. P. Menees, "Numerical simulations of an oblique detonation wave engine," *Journal of Propulsion and Power*, vol. 6, pp. 315–323, 1990. 7

[18] R. R. Bhattacharjee, "Experimental investigation of detonation re-initiation mechanisms following a mach reflection of a quenched detonation." 7, 9, 10

[19] E. Wintenberger, "Application of steady and unsteady detonation waves to propulsion," Ph.D. dissertation, California Institute of Technology, Pasadena, 2004. 8, 9

[20] M. K. Smart, "Scramjet isolators," Centre for Hypersonics, The University of Queensland, Australia. 11

[21] L. H. Quan, N. P. Hung, L. D. Quang, and V. N. Long, “Analysis and design of a scramjet engine inlet operating from mach 5 to mach 10,” *http://www.sciencepublishinggroup.com*, vol. 4, p. 11, 2 2016. [Online]. Available: http://article.sciencepublishinggroup.com/html/10.11648.j.ijmea.20160401.12.htmlhttp://www.sciencepublishinggroup.com/journal/paperinfo.aspx?journalid=220&doi=10.11648/j.ijmea.20160401.12 13

[22] T. Vanyai, M. Bricalli, S. Brieschenk, and R. R. Boyce, “Scramjet performance for ideal combustion processes,” *Aerospace Science and Technology*, vol. 75, pp. 215–226, 2018. [Online]. Available: https://www.sciencedirect.com/science/article/pii/S127096381731427X 17, 38

[23] A. Ferri, “Review of scramjet propulsion technology.” *https://doi.org/10.2514/3.43899*, vol. 5, pp. 3–10, 5 2012. [Online]. Available: https://arc.aiaa.org/doi/10.2514/3.43899 17

[24] S. Murthy and E. Curran, *Scramjet Propulsion*. American Institute of Aeronautics and Astronautics, 2001. 20

[25] F. S. Forbes and P. A. Van Splinter, “Liquid rocket propellants,” in *Encyclopedia of Physical Science and Technology (Third Edition)*, third edition ed., R. A. Meyers, Ed. New York: Academic Press, 2003, pp. 741–777. [Online]. Available: https://www.sciencedirect.com/science/article/pii/B0122274105003859 21

[26] J. P. Drummond, G. S. Diskin, and A. D. Cutler, “Chapter 6: Fuel-air mixing and combustion in scramjets,” *38th AIAA/ASME/SAE/ASEE Joint Propulsion Conference, 2006*. 30

Appendix A

Code Files

A.1 Input File

```
Master Thesis Project by Inês Pereirinha, University of Beira Interior, 2021/2022
-------------------------------------Input-----------------------------------
Altitude (m) = 0
Design Mach Number = 10
Lower Mach Number = 10
Upper Mach Number = 15
Number of shocks for compression system = 4
Desired compression ratio = 2
Ratio of specific heats for compression = 1.362
Ratio of specific heats for combustion - SCRAMJET = 1.238
Ratio of specific heats for combustion - ODWE = 1.17
Ratio of specific heats for expansion - SCRAMJET = 1.238
Ratio of specific heats for expansion - ODWE = 1.17
Specific heat at constant pressure - free-stream (J/kgK) = 1005
Specific heat at constant pressure - compression (J/kgK) = 1090
Specific heat at constant pressure - burner Scramjet (J/kgK) = 1510
Specific heat at constant pressure - burner ODWE (J/kgK) = 2000
Specific heat at constant pressure - expansion SCRAMJET (J/kgK) = 1510
Specific heat at constant pressure - expansion ODWE (J/kgK) = 2000
Ratio of fuel injection axial velocity to velocity at burner entry =0.5
Combustion Efficiency SCRAMJET= 0.9
Combustion Efficiency ODWE= 0.9
Expansion efficiency SCRAMJET= 0.9
Expansion efficiency ODWE = 0.9
Fuel definition (considering CxHy, insert x) = 0
Fuel definition (considering CxHy, insert y) = 2
Fuel Heating Value (MJ/kg) =  119.96
```

Figure A.1: Input file.

A.2 Pyhton Code

```
1  from cgi import print_arguments
2  from cmath import pi, sin, sqrt
3  from curses.ascii import SI
4  from getopt import gnu_getopt
5  from gettext import translation
6  import math
7  from posixpath import abspath
8  from re import X
9  import string
10 import sys
11 from tkinter.messagebox import YES
```

```
from tracemalloc import stop
from turtle import xcor
import numpy as np
import matplotlib.pyplot as plt
from matplotlib.backends.backend_pdf import PdfFile, PdfPages
import random
from scipy.optimize import fsolve
import warnings
warnings.simplefilter("ignore", np.ComplexWarning)

#Reading Input from input.txt file
rdm=[]
file = open("/Users/ines/Desktop/Tese/Code/input.txt","r")
lines=file.readlines()

for line in lines:
    s=''
    for c in line:
        if c.isdigit()==True:
            s1=str(c)
            s=s+s1
        if c==".":
            s1="."
            s=s+s1
    rdm.append(s)
file.close()

h=float(rdm[2])
M0=float(rdm[3])
A=int(rdm[4])
B=int(rdm[5])
x=int(rdm[6])
Tratio=float(rdm[7])
gamma_c=float(rdm[8])
gamma_b1=float(rdm[9])
gamma_b2=float(rdm[10])
gamma_e1=float(rdm[11])
gamma_e2=float(rdm[12])
Cp0=float(rdm[13])
```

```
Cpc=float(rdm[14])
Cpb1=float(rdm[15])
Cpb2=float(rdm[16])
Cpe1=float(rdm[17])
Cpe2=float(rdm[18])
VfxV4=float(rdm[19])
eta_b1=float(rdm[20])
eta_b2=float(rdm[21])
eta_e1=float(rdm[22])
eta_e2=float(rdm[23])
n_of_C=float(rdm[24])
n_of_H=float(rdm[25])
h_pr=float(rdm[26])
gamma_0=1.4
R0=-(Cp0/gamma_0)+Cp0
Rc=-(Cpc/gamma_c)+Cpc
Rb1=-(Cpb1/gamma_b1)+Cpb1
Rb2=-(Cpb2/gamma_b2)+Cpb2
Re1=-(Cpe1/gamma_e1)+Cpe1
Re2=-(Cpe2/gamma_e2)+Cpe2

if M0<8:
    print("Calculations might not be accurate, as an isolator might be
    needed for Mach < 8!")

if A<M0:
    print("This input will result in an underdriven detonation, therefore
    stable detonation cannot be assured!")
    quit()

#ISA Model
def atm(h):
    from cmath import exp, sqrt
    T_i=[288.15,216.65] #K
    P_i=[101325,22632.0637315355,5474.88855574362] #Pa
    g0=9.80665 #m/s^2
    R=287.05307 #J/kgK
    gamma=1.4
    lam=[-6.5*10**-3,1*10**-3] #K/m
```

```
88
89      #Calculation of Temperature
90      if h<11000:
91          T=T_i[0]+lam[0]*h
92      elif h<20000:
93          T=T_i[1]
94      else:
95          T=T_i[1]+lam[1]*(h-20000)
96
97      #Calculation of Pressure
98      if h<11000:
99          P=P_i[0]*(T/T_i[0])**(-g0/lam[0]/R)
100     elif h<20000:
101         P=P_i[1]*exp(-g0*(h-11000)/R/T_i[1])
102     else:
103         P=P_i[2]*(T/T_i[1])**(-g0/lam[1]/R)
104
105     #Calcualtion of Density
106     rho=P/(R*T)
107
108     #Calculation of Speed of Sound
109     a=sqrt(gamma*R*T)
110
111     #Calculation of g with altitude
112     g=g0*(6371000/(6371000+h))**2
113
114     return T,P,rho,a,g
115
116 #Function to determine properties after an oblique shock wave
117
118 def oblique(M1,theta,gamma_c,T1,P1):
119     beta=math.asin(1/M1)
120     i1=1
121     i2=0.5
122     while i1>i2:
123         a1=(2*(1/math.tan(beta)))*(M1**2*math.sin(beta)**2-1)
124         a2=(M1**2*(gamma_c+math.cos(2*beta)))+2
125         i1=abs(math.tan(theta)-a1/a2)
126         beta+=0.00001
```

```
        a3=(2*(1/math.tan(beta)))*(M1**2*math.sin(beta)**2-1)
        a4=(M1**2*(gamma_c+math.cos(2*beta)))+2
        i2=abs(math.tan(theta)-a3/a4)
    beta=beta-0.00001
    i=M1*math.sin(beta)
    if abs(i)<1.0:
        print("At this wave angle, no oblique shock wave is possible")
        quit()
    rhoratio=((gamma_c+1)*(M1**2*math.sin(beta)**2))/(2+(gamma_c-1)*M1**2*
    math.sin(beta)**2)
    Pratio=1+(2*gamma_c)/(gamma_c+1)*(M1**2*math.sin(beta)**2-1)
    Tratio=Pratio/rhoratio
    T2=Tratio*T1
    P2=Pratio*P1
    M2=2/(gamma_c-1)
    M2=M2*((1/Tratio)*(1+((gamma_c-1)/2)*M1**2)-1)
    M2=sqrt(M2)
    return abs(M2),T2,P2

#Inlet Design
T0,P0,rho,a,g0=atm(h)
theta=math.radians(1)
while theta<1:
    #1st compression shock
    beta=math.asin(1/M0)
    i1=(2*(M0**2*math.sin(beta)**2-1))
    i2=(math.tan(beta)*((M0**2*(gamma_c+math.cos(2*beta))+2)))
    while abs(math.tan(theta)-(i1/i2))>0.0001:
        beta=beta+0.0001
        i1=(2*(M0**2*math.sin(beta)**2-1))
        i2=(math.tan(beta)*((M0**2*(gamma_c+math.cos(2*beta))+2)))
    pratio=abs(1+(2*gamma_c/(gamma_c+1))*(abs(M0**2*math.sin(beta)**2-1)))
    e=pratio
    rhoratio=abs((M0**2*math.sin(beta)**2*(gamma_c+1))/(2+(gamma_c-1)*M0
    **2*math.sin(beta)**2))
    M1=abs(sqrt((2/(gamma_c-1))*((rhoratio/pratio)*(1+((gamma_c-1)/2)*M0
    **2)-1)))
    a=abs(pratio/rhoratio)

```

```
    #2nd compression shock
    beta=math.asin(1/M1)
    i1=(2*(M1**2*math.sin(beta)**2-1))
    i2=(math.tan(beta)*((M1**2*(gamma_c+math.cos(2*beta))+2)))
    while abs(math.tan(theta)-(i1/i2))>0.0001:
        beta=beta+0.0001
        i1=(2*(M1**2*math.sin(beta)**2-1))
        i2=(math.tan(beta)*((M1**2*(gamma_c+math.cos(2*beta))+2)))
    pratio=1+(2*gamma_c/(gamma_c+1))*(abs(M1**2*math.sin(beta)**2-1))
    f=pratio
    rhoratio=(M1**2*math.sin(beta)**2*(gamma_c+1))/(2+(gamma_c-1)*M1**2*
    math.sin(beta)**2)
    M2=abs(sqrt((2/(gamma_c-1))*((rhoratio/pratio)*(1+((gamma_c-1)/2)*M1
    **2)-1)))
    b=abs(pratio/rhoratio)

    #3rd compression shock
    beta=math.asin(1/M2)
    i1=(2*(M2**2*math.sin(beta)**2-1))
    i2=(math.tan(beta)*((M2**2*(gamma_c+math.cos(2*beta))+2)))
    while abs(math.tan(theta)-(i1/i2))>0.0001:
        beta=beta+0.0001
        i1=(2*(M2**2*math.sin(beta)**2-1))
        i2=(math.tan(beta)*((M2**2*(gamma_c+math.cos(2*beta))+2)))
    pratio=1+(2*gamma_c/(gamma_c+1))*(abs(M2**2*math.sin(beta)**2-1))
    g=pratio
    rhoratio=(M2**2*math.sin(beta)**2*(gamma_c+1))/(2+(gamma_c-1)*M2**2*
    math.sin(beta)**2)
    M3=abs(sqrt((2/(gamma_c-1))*((rhoratio/pratio)*(1+((gamma_c-1)/2)*M2
    **2)-1)))
    c=pratio/rhoratio

    #4th compression shock
    beta=math.asin(1/M3)
    i1=(2*(M3**2*math.sin(beta)**2-1))
    i2=(math.tan(beta)*((M3**2*(gamma_c+math.cos(2*beta))+2)))
    while abs(math.tan(theta)-(i1/i2))>0.0001:
        beta=beta+0.00001
        i1=(2*(M3**2*math.sin(beta)**2-1))
```

```
        i2=(math.tan(beta)*((M3**2*(gamma_c+math.cos(2*beta))+2)))
    pratio=1+(2*gamma_c/(gamma_c+1))*(abs(M3**2*math.sin(beta)**2-1))
    h=pratio
    rhoratio=(M3**2*math.sin(beta)**2*(gamma_c+1))/(2+(gamma_c-1)*M3**2*
    math.sin(beta)**2)
    M4=abs(sqrt((2/(gamma_c-1))*((rhoratio/pratio)*(1+((gamma_c-1)/2)*M3
    **2)-1)))
    d=pratio/rhoratio

    attempt=abs(d*c*b*a-Tratio)
    if abs(attempt)<0.01:
        tpratio=e*f*g*h*((1/(a*b*c*d)))**(gamma_c/(gamma_c-1))
        eta_c=a*b*c*d-(1/tpratio)**((gamma_c-1)/gamma_c)
        eta_c=eta_c/(a*b*c*d-1)
        eta_ke=1-(2/((gamma_c-1)*M0**2))*(-1+(1/tpratio)**((gamma_c-1)/
    gamma_c))
        break
    theta=theta+0.001

#Determination of ODWE wedge angle for Ch.J detonation
f=(36*n_of_C+3*n_of_H)/(412*n_of_C+103*n_of_H)
Q=(((h_pr*10**6)*f)/(f+1))*eta_b2
T4=a*b*c*d*T0
Q_bar=Q/(Cpc*T4)
V4=abs(M4*sqrt(gamma_c*(Rc)*T4))
V4=V4*((1+f*VfxV4)/(1+f))
M4=M4*((1+f*VfxV4)/(1+f))

def ChJ(var):
    x=var
    eq1 = ((M4*math.sin(x))**2-1)**2-2*(gamma_c+1)*((M4*math.sin(x))**2)*
    Q_bar
    return eq1
beta=  fsolve(ChJ,((math.asin(1/M4)+1)))
if math.asin(1/M4)>beta>(pi/2):
    print("ERROR with detonation angle! Angle must be between",math.degrees
    (math.asin(1/M4)),"and 90 degrees")
i=(M4*math.sin(beta))**2
wedge_angle=beta-math.atan((1+gamma_c*i)/((gamma_c+1)*i*abs(sqrt((M4/sqrt(i
```

```
    ))**2-1))))

#Determination of Properties after the compression system
i=0
matrix = [ [ 0 for y in range( 4 ) ] for x in range( (B-A)+1 ) ]
for M in range(A,B+1,1):
    T1=T0
    P1=P0
    M1=M
    for n_of_shocks in range (1,5,1):
        M2,T2,P2=oblique(M1,theta,gamma_c,T1,P1)
        if abs(M2)<1:
            print("ERROR: Supersonic combustion is not possible!")
            quit()
        if  T2>1000:
            print("Preignition can occur!")
        M1=M2
        T1=T2
        P1=P2
    matrix[i][0]=M2
    matrix[i][1]=T2
    matrix[i][2]=P2
    matrix[i][3]=M
    i=i+1

#Scramjet Combustion
#Constant Pressure
def combustion_scramjet(T1,Cpb,f,h_pr,M1):
    V1=abs(M1*sqrt(gamma_c*(Rc)*T1))
    V2=V1*((1+f*VfxV4)/(1+f))
    T2=(T1/(1+f))*(1+(1/(Cpb*T1))*(eta_b1*f*h_pr*10**6+f*Cpb*222+(1+f*(
    VfxV4)**2)*((V1**2)/2)))-((V2**2)/(2*Cpb))
    return T2,V2

T_pb1 = [ [ 0 for y in range( 2 ) ] for x in range( (B-A)+1 ) ]
for i in range(0,(B-A)+1,1):
    T_pb1[i][0],T_pb1[i][1]=combustion_scramjet(matrix[i][1],Cpb1,f,h_pr,
    matrix[i][0])

```

```
#Constant Area
def combustion_scramjetca(T1,Cpb,f,h_pr,M1,P1):
    V1=abs(M1*sqrt(gamma_c*(Rc)*T1))
    a=1-(Rb1/(2*Cpb))
    b=(-V1/(1+f))*(f*VfxV4+(1+((Rb1*T1)/(V1**2))))
    c=(1+(1/(Cpb*T1))*(eta_b1*f*h_pr*10**6+f*Cpb*222+(1+f*(VfxV4)**2)*((V1
    **2)/2)))*((Rb1*T1)/(1+f))
    V2=(-b+abs(sqrt(b**2-4*a*c)))/(2*a)
    T2=(c/Rb1)-((V2**2)/(2*Cpb))
    P2=P0*(1+f)*(T2/T1)*(V1/V2)*(P1/P0)
    return T2,V2,P2

T_pb1ca = [ [ 0 for y in range( 3 ) ] for x in range( (B-A)+1 ) ]
for i in range(0,(B-A)+1,1):
    T_pb1ca[i][0],T_pb1ca[i][1],T_pb1ca[i][2]=combustion_scramjetca(matrix[
    i][1],Cpb1,f,h_pr,matrix[i][0],matrix[i][2])


#Expansion Scramjet
def expansion(T1,P1,V1,eta_e,R,Cp,f,M0,T0,P0):
    #1 is 4 and 2 is to 10
    V0=abs(M0*sqrt(gamma_0*(R0)*T0))
    T2=T1*(1-eta_e*(1-(P0/P1)**(R/Cp)))
    V2=abs(sqrt(V1**2+2*Cp*(T1-T2)))
    P2=P0
    Aratio=(1+f)*(T2/T0)*(V0/V2)
    return Aratio,T2,P2,V2

Station10_1 = [ [ 0 for y in range( 4 ) ] for x in range( (B-A)+1 ) ]
for i in range(0,(B-A)+1,1):
    Station10_1[i][0],Station10_1[i][1],Station10_1[i][2],Station10_1[i
    ][3]=expansion(T_pb1[i][0],matrix[i][2],T_pb1[i][1],eta_e1,Re1,Cpe1,f,
    matrix[i][3],T0,P0)

Station10_1ca = [ [ 0 for y in range( 4 ) ] for x in range( (B-A)+1 ) ]
for i in range(0,(B-A)+1,1):
    Station10_1ca[i][0],Station10_1ca[i][1],Station10_1ca[i][2],
    Station10_1ca[i][3]=expansion(T_pb1ca[i][0],T_pb1ca[i][2],T_pb1ca[i
    ][1],eta_e1,Re1,Cpe1,f,matrix[i][3],T0,P0)
```

```
301
302
303 #ODWE Combustion
304 def post_detonation(P1,T1,rho1,V1,theta,Cp,M1,Q):
305     M1=M1*((1+f*VfxV4)/((1+f)))
306     def first_root(var):
307         x=var
308         eq1=(-(gamma_c+1)/2)*(math.tan(x-theta)/math.tan(x))**2*(M1**2)*(
    math.sin(x)**2)+(math.tan(x-theta)/math.tan(x))*(1+gamma_c*(M1**2)*(
    math.sin(x)**2))-(1+((gamma_c-1)/2)*(M1**2)*(math.sin(x)**2))-Q
309         return eq1
310     beta=fsolve(first_root,(math.asin(1/M1)))
311     X=math.tan(beta-theta)/math.tan(beta)
312     V1=abs(M1*sqrt(Rc*T1*gamma_c))
313     V1=V1*math.sin(beta)
314     P2=P1+rho1*(V1**2)*(1-X)
315     Tratio=1+((V1**2)/(2*Cp*T1))*(1-X**2)+(Q)
316     T2=Tratio*T1
317     V2=(V1*X)/(math.sin(beta-theta))
318     M2=abs(V2/sqrt(gamma_b2*Rb2*T2))
319     if M2<1:
320         print("Warning - Detonation can be unstable!")
321     M2n=abs((V1*X)/sqrt(gamma_b2*Rb2*T2))
322     return T2,P2,V2
323
324 T_pb2 = [ [ 0 for y in range( 3 ) ] for x in range( (B-A)+1 ) ]
325 for i in range(0,(B-A)+1,1):
326     rho=(matrix[i][2])/(Rc*matrix[i][1])
327     Q=(((h_pr*10**6)*f)/(f+1)/(Cpc*matrix[i][1]))*eta_b2
328     T_pb2[i][0],T_pb2[i][1],T_pb2[i][2]=post_detonation(matrix[i][2],matrix
    [i][1],rho,matrix[i][0],wedge_angle,Cpc,matrix[i][0],Q)
329
330 #Expansion ODWE
331 Station10_2 = [ [ 0 for y in range( 4 ) ] for x in range( (B-A)+1 ) ]
332 for i in range(0,(B-A)+1,1):
333     Station10_2[i][0],Station10_2[i][1],Station10_2[i][2],Station10_2[i
    ][3]=expansion(T_pb2[i][0],T_pb2[i][1],T_pb2[i][2],eta_e2,Re2,Cpe2,f,
    matrix[i][3],T0,P0)
334
```

```
#Performance
def performance(R1,R2,V10,T10,V0,Aratio,f,g):
    Ve=V10
    Sa10=V10+((R2*T10)/V10)
    Sa0=V0+((R1*T0)/V0)
    st=(1+f)*Sa10-Sa0-((R1*T0)/V0)*(Aratio-1)
    sfc=f/st
    si=1/(g0*sfc)
    Vratio=Ve/V0
    eta_p=2/(Vratio+1)
    eta_th=((((1+f)*(Ve**2)/2)-((V0**2)/2)))/(f*h_pr*1000000)
    eta_o=eta_th*eta_p
    return st,sfc,si,eta_p,eta_th,eta_o

per_scramjet = [ [ 0 for y in range( 6 ) ] for x in range( (B-A)+1 ) ]
per_scramjetca = [ [ 0 for y in range( 6 ) ] for x in range( (B-A)+1 ) ]
per_ODWE = [ [ 0 for y in range( 6 ) ] for x in range( (B-A)+1 ) ]

for i in range(0,(B-A)+1,1):
    V0=abs(matrix[i][3]*sqrt(T0*gamma_0*R0))
    per_scramjet[i][0],per_scramjet[i][1],per_scramjet[i][2],per_scramjet[i
    ][3],per_scramjet[i][4],per_scramjet[i][5]=performance(R0,Re1,
    Station10_1[i][3],Station10_1[i][1],V0,Station10_1[i][0],f,g0)
    per_scramjetca[i][0],per_scramjetca[i][1],per_scramjetca[i][2],
    per_scramjetca[i][3],per_scramjetca[i][4],per_scramjetca[i][5]=
    performance(R0,Re1,Station10_1ca[i][3],Station10_1ca[i][1],V0,
    Station10_1ca[i][0],f,g0)
    per_ODWE[i][0],per_ODWE[i][1],per_ODWE[i][2],per_ODWE[i][3],per_ODWE[i
    ][4],per_ODWE[i][5]=performance(R0,Re2,Station10_2[i][3],Station10_2[i
    ][1],V0,Station10_2[i][0],f,g0)

#Plotting Results
Mach=[]
Mach=[0 for i in range((B-A)+1)]
ST_SCRAMJET=[]
ST_SCRAMJET=[0 for i in range((B-A)+1)]
ST_SCRAMJETca=[]
ST_SCRAMJETca=[0 for i in range((B-A)+1)]
ST_ODWE=[]
```

```
ST_ODWE=[0 for i in range((B-A)+1)]
SFC_SCRAMJET=[]
SFC_SCRAMJET=[0 for i in range((B-A)+1)]
SFC_SCRAMJETca=[]
SFC_SCRAMJETca=[0 for i in range((B-A)+1)]
SFC_ODWE=[]
SFC_ODWE=[0 for i in range((B-A)+1)]
SI_SCRAMJET=[]
SI_SCRAMJET=[0 for i in range((B-A)+1)]
SI_SCRAMJETca=[]
SI_SCRAMJETca=[0 for i in range((B-A)+1)]
SI_ODWE=[]
SI_ODWE=[0 for i in range((B-A)+1)]
ETA_p_SCRAMJET=[]
ETA_p_SCRAMJET=[0 for i in range((B-A)+1)]
ETA_p_SCRAMJETca=[]
ETA_p_SCRAMJETca=[0 for i in range((B-A)+1)]
ETA_p_ODWE=[]
ETA_p_ODWE=[0 for i in range((B-A)+1)]
ETA_th_SCRAMJET=[]
ETA_th_SCRAMJET=[0 for i in range((B-A)+1)]
ETA_th_SCRAMJETca=[]
ETA_th_SCRAMJETca=[0 for i in range((B-A)+1)]
ETA_th_ODWE=[]
ETA_th_ODWE=[0 for i in range((B-A)+1)]
ETA_o_SCRAMJET=[]
ETA_o_SCRAMJET=[0 for i in range((B-A)+1)]
ETA_o_SCRAMJETca=[]
ETA_o_SCRAMJETca=[0 for i in range((B-A)+1)]
ETA_o_ODWE=[]
ETA_o_ODWE=[0 for i in range((B-A)+1)]
Aratiocp=[]
Aratiocp=[0 for i in range((B-A)+1)]
Aratioca=[]
Aratioca=[0 for i in range((B-A)+1)]
AratioODWE=[]
AratioODWE=[0 for i in range((B-A)+1)]

for i in range(0,(B-A)+1,1):
```

```
    Mach[i]=matrix[i][3]
    ST_SCRAMJET[i]=per_scramjet[i][0]
    SFC_SCRAMJET[i]=per_scramjet[i][1]
    ST_SCRAMJETca[i]=per_scramjetca[i][0]
    SFC_SCRAMJETca[i]=per_scramjetca[i][1]
    SI_SCRAMJET[i]=per_scramjet[i][2]
    ETA_p_SCRAMJET[i]=per_scramjet[i][3]
    ETA_th_SCRAMJET[i]=per_scramjet[i][4]
    ETA_o_SCRAMJET[i]=per_scramjet[i][5]
    SI_SCRAMJETca[i]=per_scramjetca[i][2]
    ETA_p_SCRAMJETca[i]=per_scramjetca[i][3]
    ETA_th_SCRAMJETca[i]=per_scramjetca[i][4]
    ETA_o_SCRAMJETca[i]=per_scramjetca[i][5]
    ST_ODWE[i]=per_ODWE[i][0]
    SFC_ODWE[i]=per_ODWE[i][1]
    SI_ODWE[i]=per_ODWE[i][2]
    ETA_p_ODWE[i]=per_ODWE[i][3]
    ETA_th_ODWE[i]=per_ODWE[i][4]
    ETA_o_ODWE[i]=per_ODWE[i][5]
    Aratiocp[i]=Station10_1[i][0]
    Aratioca[i]=Station10_1ca[i][0]
    AratioODWE[i]=Station10_2[i][0]

#PLOTTING SPECIFIC THRUST VS. FREESTREAM MACH NUMBER

with PdfPages("/Users/ines/Desktop/Tese/Code/output.pdf") as pdf:
    x = Mach
    y=ST_SCRAMJET
    z = ST_ODWE
    w=ST_SCRAMJETca
    plt.plot(x, y,'r',label="Scramjet Constant Pressure")
    plt.plot(x, z,'b',label="ODWE")
    plt.plot(x, w,'g',label="Scramjet Constant Area")
    plt.xlabel('Freestream Mach Number, $M_0$')
    plt.ylabel('Specific Thrust, [$Ns/kg$]')
    plt.legend()
    pdf.savefig()
    plt.show()
    plt.close()
```

```
445
446
447 #PLOTTING SPECIFIC FUEL CONSUMPTION VS. FREESTREAM MACH NUMBER
448     x = Mach
449     y=SFC_SCRAMJET
450     z = SFC_ODWE
451     w=SFC_SCRAMJETca
452     plt.plot(x, y,'r',label="Scramjet Constant Pressure")
453     plt.plot(x, z,'b',label="ODWE")
454     plt.plot(x, w,'g',label="Scramjet Constant Area")
455     plt.xlabel('Freestream Mach Number, $M_0$')
456     plt.ylabel('Specific Fuel Consumption, [$kg/Ns$]')
457     plt.ticklabel_format(axis="y",style='sci',scilimits=(0,0))
458     plt.legend()
459     pdf.savefig()
460     plt.show()
461     plt.close()
462
463
464 #PLOTTING SPECIFIC IMPULSE VS. FREESTREAM MACH NUMBER
465     x = Mach
466     y=SI_SCRAMJET
467     z = SI_ODWE
468     w=SI_SCRAMJETca
469     plt.plot(x, y,'r',label="Scramjet Constant Pressure")
470     plt.plot(x, z,'b',label="ODWE")
471     plt.plot(x, w,'g',label="Scramjet Constant Area")
472     plt.xlabel('Freestream Mach Number, $M_0$')
473     plt.ylabel('Specific Impulse, $I_{sp}\,[s]$ ')
474     plt.legend()
475     pdf.savefig()
476     plt.show()
477     plt.close()
478
479
480 #PLOTTING PROPULSIVE EFFICIENCY VS. FREESTREAM MACH NUMBER
481     x = Mach
482     y = ETA_p_SCRAMJET
483     z=ETA_p_ODWE
```

```
    w=ETA_p_SCRAMJETca
    plt.plot(x, y,'r',label="Scramjet Constant Pressure")
    plt.plot(x, z,'b',label="ODWE")
    plt.plot(x, w,'g',label="Scramjet Constant Area")
    plt.xlabel('Freestream Mach Number, $M_0$')
    plt.ylabel('Propulsive Efficiency, $eta_p$ ')
    plt.legend()
    pdf.savefig()
    plt.show()
    plt.close()


#PLOTTING THERMAL EFFICIENCY VS. FREESTREAM MACH NUMBER
    x = Mach
    y = ETA_th_SCRAMJET
    z= ETA_th_ODWE
    w=ETA_th_SCRAMJETca
    plt.plot(x, y,'r',label="Scramjet Constant Pressure")
    plt.plot(x, z,'b',label="ODWE")
    plt.plot(x, w,'g',label="Scramjet Constant Area")
    plt.xlabel('Freestream Mach Number, $M_0$')
    plt.ylabel('Thermal Efficiency, $eta_{th}$ ')
    plt.legend()
    pdf.savefig()
    plt.show()
    plt.close()


#PLOTTING GLOBAL EFFICIENCY VS. FREESTREAM MACH NUMBER
    x = Mach
    y = ETA_o_SCRAMJET
    z=ETA_o_ODWE
    w=ETA_o_SCRAMJETca
    plt.plot(x, y,'r',label="Scramjet Constant Pressure")
    plt.plot(x, z,'b',label="ODWE")
    plt.plot(x, w,'g',label="Scramjet Constant Area")
    plt.xlabel('Freestream Mach Number, $M_0$')
    plt.ylabel('Overall Efficiency, $eta_o$ ')
    plt.legend()
```

```
    pdf.savefig()
    plt.show()
    plt.close()


#PLOTTING A10/A0 VS. FREESTREAM MACH NUMBER
    x = Mach
    y = Aratiocp
    z=Aratioca
    w=AratioODWE
    plt.plot(x, y,'r',label="Scramjet Constant Pressure")
    plt.plot(x, w,'b',label="ODWE")
    plt.plot(x, z,'g',label="Scramjet Constant Area")
    plt.xlabel('Freestream Mach Number, $M_0$')
    plt.ylabel('A10/A0')
    plt.legend()
    pdf.savefig()
    plt.show()
    plt.close()
```